Proteomics Identifies Osteomodulin as a Promoter of Breast Cancer Bone Metastasis via CDK1 Activation

Sara Cabral[1,8,*], Joseph Parsons[1,2,*], Hannah Harrison[1,8], Thomas Kedward[1,8], Paul Fullwood[2], Katherine Spence[1,8], Diane V. Lefley[3], Danielle Barden[2], Jennifer Ferguson[2], Joanne Watson[2], Kalliopi Tsafou[4], Caron Behan[5], Mark J. Dunning[6], Nisha Ali[7,8], Balázs Győrffy[9,10,11], Janet Brown[3], Michael P. Smith[2], Penelope D. Ottewell[3], Ciara S. O'Brien[1,8,12,**] Chiara Francavilla[2,8,13,**,#], Robert B. Clarke[1,8,**,#]

[1]Division of Cancer Sciences, School of Medical Sciences, Faculty of Biology Medicine and Health, University of Manchester, Manchester UK

[2]Division of Cellular and Molecular Function, School of Biological Sciences, Faculty of Biology Medicine and Health, University of Manchester, Manchester, UK

[3]Division of Clinical Medicine, Medical School, University of Sheffield, Sheffield, UK

[4]Stanley Center for Psychiatric Research, Broad Institute of MIT and Harvard, Cambridge, MA, USA

[5]Histology Cancer Research UK Manchester Institute, Manchester, UK

[6]Sheffield Bioinformatics Core, School of Medicine and Population Health, University of Sheffield, UK

[7]Manchester University Foundation Trust, Wythenshawe Hospital, Manchester, UK

[8]Manchester Breast Centre, University of Manchester, Manchester, UK

[9]Department of Bioinformatics, Semmelweis University, H-1094, Budapest, Hungary

[10]Department of Biophysics, Medical School, University of Pecs, H-7624, Pecs, Hungary

[11]Institute of Molecular Life Sciences, HUN-REN Research Centre for Natural Sciences, H-1117, Budapest, Hungary

[12]Department of Medical Oncology, Christie Hospital, Manchester, UK

[13]DTU Bioengineering, Danish Technical University, Lyndby, Denmark

*Equal Contribution

**Equal Senior Contribution

#Corresponding Authors:

Chiara Francavilla: chiafra@dtu.dk

Robert Clarke: robert.clarke@manchester.ac.uk

Keywords: breast cancer, stroma, bone metastasis, proteomics, phosphoproteomics, osteomodulin, CDK1, CDK1 inhibitor, cancer-associated fibroblasts

Summary

Metastasis to different organs remains the main cause of mortality in breast cancer. Molecular predictors of metastasis are limited as well as therapeutic options. Here, we conducted quantitative proteomics and phosphoproteomics analysis of patient-derived tumours, identifying osteomodulin (OMD) as a dysregulated protein and associated with bone metastases. Cancer-associated fibroblasts secrete OMD which increases breast cancer migration *in vitro* and promotes the formation of bone metastases *in vivo*. Downstream of OMD, phosphoproteomics identified the activation of cyclin-dependent kinase 1 (CDK1). The OMD-CDK1 signalling axis drives a pro-migratory and pro-survival phenotype *in vitro* and bone metastasis *in vivo*. Our findings highlight the importance of OMD and CDK1 in breast cancer bone metastasis and proposes an alternative therapeutic avenue for the treatment and the prevention of organ-specific metastases.

45 ## Introduction

46 Metastases are responsible for 90% of breast cancer deaths [1] and are most commonly found
47 in the bone, brain, liver and lungs of breast cancer patients [2]. Bone is the most prevalent site
48 of metastasis, representing around 70% of metastatic breast cancers cases[3]. Bone
49 metastases are characterized by being mainly osteolytic, leading to debilitating symptoms
50 such as pathological fractures, severe bone pain, and hypercalcemia[4]. Currently, there are no
51 clinically available biomarkers nor targeted drug therapies against organ-specific metastases
52 in breast despite the identification of different drivers of metastatic disease[3]. Radiologically
53 detected, or symptomatic bone metastases are typically managed with bisphosphonates and
54 receptor activator of NF-κB ligand (RANKL) inhibitors to alleviate symptoms and reduce bone
55 osteolysis[4]. However, there is still the need to uncover more specific biomarkers and
56 actionable combinations of therapeutic targets for patients at risk of developing metastases.
57 Preventing bone metastasis or targeting bone organotropic drivers would greatly benefit
58 patients given the capacity of the bone microenvironment to condition tumour cells to colonise
59 other organs [5-7].

60 Omics technologies have the capacity to provide novel biomarkers and therapeutic targets
61 from a variety of tissues, including patient-derived samples [8]. For instance, genomic analysis
62 of metastatic breast cancer patient samples or matched primary and metastatic breast cancer
63 patient samples identified several potential therapeutic targets whose mutation was enriched
64 in metastases [9]. Transcriptomic analysis of breast cancer primary and metastatic samples also
65 identified several transcripts dysregulated in breast cancer bone metastases compared to
66 other metastatic sites [10]. In contrast to genomics and transcriptomics, proteomics and
67 phosphoproteomics have so far analysed primary breast cancer but not metastatic samples
68 [11], for example identifying dysregulation in tumour cells metabolism [12], novel kinases in triple
69 negative breast cancer patients [13], and signalling pathways associated with Epidermal Growth
70 Factor Receptor 2 (HER2)-targeted therapy resistance [14].

71 Here, we set out to identify potential therapeutic targets and their biomarkers in breast cancer
72 metastasis organotropism. Fresh frozen primary breast cancer resection samples that were
73 clinically annotated as to the presence or absence of organ-specific metastases within 5 years
74 of diagnosis (distant disease-free survival at 5 years) were analysed. We combined mass
75 spectrometry-based proteomics and phosphoproteomics, bioinformatics, and functional
76 assays *in vitro* and *in vivo*. This experimental pipeline identified Osteomodulin (OMD), a
77 secreted member of the small leucine-rich proteoglycan family typically expressed by
78 osteoblasts and associated with biomineralization processes[15,16]. We demonstrated that OMD
79 is expressed and secreted by cancer-associated fibroblasts (CAFs) and stimulates the
80 migration of estrogen receptor-positive (ER+) and ER-negative breast cancer cells. Using
81 further phosphoproteomic analysis of OMD-stimulated breast cancer cells, we identified
82 activation of Cyclin-dependent kinase (CDK1) to be necessary for BC migration, viability and
83 bone metastasis. High OMD and CDK1 co-expression predicts metastatic outcome
84 independently of other clinical and prognostic factors in a large cohort of breast cancer with
85 over 15 years follow-up. Overall, this research establishes CAF-derived OMD and
86 downstream CDK1 signalling as important regulator of breast cancer metastasis to the bone.

87 ## Results

88 ### Proteomic Analysis of Primary Breast Cancer Samples Identifies Osteomodulin (OMD)
89 in Patients Developing Bone Metastases

90 To identify changes in proteins and phosphorylated proteins underlying breast cancer
91 metastasis, we analysed a cohort of 39 primary breast cancer patient samples, of which 21
92 developed metastases within 5 years of diagnosis (here, referred to as metastatic) while 18
93 were distant disease free at 5 years (here, referred to as non-metastatic), by label-free mass
94 spectrometry-based proteomics and phosphoproteomics (Figure 1A, Tables S1-3). Of the 39
95 patient samples, 21 were from patients who had hormone receptor positive (HR+) tumours, 9
96 who had human epidermal growth factor receptor 2 positive (HER2+) tumours and 9 who had

97 triple negative (TN) tumours. Our cohort included patients who developed metastases at all
98 four of the main metastatic sites in breast cancer at 5 years post-diagnosis (bone, brain, liver
99 and lung) [2], thus providing a unique dataset (Figure 1A, Table S1). We identified and quantified
100 a total of 6243 proteins (5106 in non-metastatic samples and 5741 in metastatic samples) and
101 14281 phosphorylated sites (11148 in non-metastatic samples and 13186 in metastatic
102 samples) (Figure S1A-B, Tables S2-3). Pearson correlation for technical replicates in the
103 proteomics data was above 0.95 on average and was above 0.6 on average in the
104 phosphoproteomics data (Figure S1C-D), thus showing high correlation. Across
105 phosphorylated sites, 62.8% were singly phosphorylated, 29.0% were doubly phosphorylated
106 and 7.2% were more than doubly phosphorylated and the residue distribution across serine,
107 threonine and tyrosine was 88.24%, 10.92%, 0.83%, respectively with a median score for
108 phosphorylated peptides of 172 (Figure S1E-G). Therefore, the quality of our proteomics and
109 phosphoproteomics analysis was consistent with previous publications [11,17].

110 We focused on proteins and phosphorylated sites present in at least 80% of either non-
111 metastatic or metastatic samples for further analysis (Tables S4-5). Differential expression
112 analysis of patients who developed or did not develop metastases identified 33 differentially
113 regulated proteins and 156 differentially regulated phosphorylated sites on 122 proteins (p
114 value <0.05, Log2 Fold Change in intensity >1.5) (Figure 1B-C, Tables S4-5). To determine
115 whether these differentially regulated proteins and phosphorylated sites had previously been
116 associated with breast cancer metastasis, we compared our list of 33 dysregulated proteins
117 and 156 dysregulated phosphorylated sites with an in-house curated database of metastasis-
118 associated genes and proteins obtained by searching PubMed with the term “Breast Cancer
119 Metastasis” for a total of 2472 entries (Table S6). We found that ADIRF, CMA1, COL11A1,
120 COL4A1, CTHRC1, MXRA5, OGN, OMD, SNCG, SYNM, TNC proteins and BAD, MAPK1 (2
121 sites), PGRMC1 (2 sites), STMN1, EIF4B and VIM phosphorylated sites have been previously
122 associated with breast cancer metastasis or metastasis-promoting phenotypes (Figure 1B-C,

123 Tables S4-6). Thus, our proteomics and phosphoproteomics analysis identified both known
124 and novel drivers of breast cancer metastasis.

125 Next, KEGG and GO enrichment analysis identified several biological processes among all
126 the upregulated proteins and phosphoproteins, including collagen remodelling, previously
127 associated with breast cancer [18] (Figure 1D, Table S7). Osteomodulin (OMD), a member of
128 the small leucine-rich repeat protein family[15,16], was among the upregulated proteins and
129 phosphorylated sites associated with collagen synthesis and remodelling. Analysis of
130 published datasets had previously found OMD gene expression to be correlated with breast
131 cancer bone metastasis[10]. In our study, OMD protein was found to be significantly higher in
132 patients who developed bone metastasis compared to patients who developed metastases in
133 other sites (*p* value = 0.0012), or that did not develop metastases (*p* value = <0.0001) (Figure
134 1E, Tables S1, S4). Immunohistochemical analysis of the primary tumour from the same
135 cohort of breast cancer samples detected OMD in 17 samples and showed heterogeneous
136 staining in the tumour and stromal compartments (Figure S2). Consistent with OMD protein
137 expression being associated with bone metastasis, we found that OMD mRNA was
138 significantly higher in patients developing bone metastases compared to other metastatic sites
139 based on three published breast cancer GEO datasets (Figure 1F) [10,19].

140 Overall, our proteomic and immunohistochemical analysis of primary breast cancer samples
141 indicates that OMD expression is higher in breast cancer patients developing bone metastasis.

142 **OMD is Expressed by Cancer-Associated Fibroblasts and Regulates Cell Migration in**
143 **HR+ and HR- Breast Cancer**

144 As OMD was found in the tumour and in its microenvironment (Figure S2), we first tested
145 whether OMD affected either cells in the tumour microenvironment or the epithelial tumour
146 cells themselves. We used cell models of the primary and secondary (bone) tumour
147 microenvironment including normal and cancer-associated fibroblasts (CAFs) (HMFU19 and
148 544R, respectively) [20,21], osteoblasts (HFOB 1.19) [22], and osteoclasts (RAW 264.7, post-

149 differentiation with RANKL) [23]. As a model of tumour epithelial cells, we used the epithelial
150 breast cancer cell line MDA-MB-231 infected with lentivirus expressing either mApple as a
151 control (231-mA) or an OMD-T2A linker-mApple construct (231-OMD) (Figure 2A-B). OMD
152 expression was confirmed by immunoblotting in cell lysates from both starvation and complete
153 media and in conditioned medium (CM) (Figure 2A-B), thus confirming that OMD is a secreted
154 protein [24]. We tested whether there were any effects on osteogenesis, a key process in the
155 differentiation and turnover of bone tissues involved in sclerotic metastases [25], by assessing
156 Alkaline Phosphatase Activity and calcium deposition via Alizarin Red staining. To mimic
157 secreted OMD, we used recombinant OMD (rOMD) at increasing concentrations from 10ng/ml
158 to 1µg/ml, which recapitulates the concentrations used by others[26]. Both osteogenesis and
159 calcium deposition were significantly induced in the osteoblast cells upon differentiation
160 (Figure S3A-C). However, compared to differentiated osteoblasts, alkaline phosphatase
161 activity is unaffected by conditioned medium (CM) from 231-mA or 231-OMD or by increasing
162 concentrations of rOMD, except for the highest concentration of rOMD which induces calcium
163 deposition. Additionally, in the bone-resorbing osteoclasts, no significant induction of activity
164 was seen upon treatment of osteoclasts with either CM from 231-mA and from 231-OMD cells
165 or rOMD was observed, as the number and size of pores was consistent across all conditions
166 (Figure 2A-B, Figure S3D-G). Collagen contractility was also assessed to understand whether
167 OMD affects matrix remodelling in normal fibroblasts, CAFs and differentiated osteoblasts.
168 rOMD and CM derived from 231-OMD and 231-mA cells had no effect on the collagen
169 remodelling capabilities of each of the tested cells (Figure S3H-J).

170 Using 231-OMD cells, we next tested whether OMD expression affected the behaviour of
171 breast cancer cells. We assessed behaviour by looking at effects on extracellular matrix
172 remodelling, proliferation and stemness of breast cancer cells by conducting collagen
173 contractility assays, measuring EdU incorporation, and mammosphere formation and self-
174 renewal assays, respectively. We found that OMD overexpression had no effects on any of
175 these behaviours (Figure S4A-D). We next assessed the effects of OMD on cell migration

176 using a scratch wound assay and cell invasion using a Boyden chamber assay. Although
177 invasion was not significantly altered between 231-mA and 231-OMD cells in our experimental
178 conditions, OMD expression significantly increased cell migration (Figure 3C-D, Figure S4E).
179 Additionally, treatment with increasing concentrations of rOMD significantly induced 231-mA
180 cell migration in a dose-dependent manner (Figure 3C-D). We also tested the effect of rOMD
181 on the migration of ER+ MCF-7 cell line (Fig 3F-G), and confirmed that the highest
182 concentration of rOMD increased MCF-7 migration. However, OMD expression did not affect
183 cell motility of the bone-tropic MDA-MB-231 (231-Bo) cell line [27]. Indeed, cell migration of the
184 bone-tropic MDA-MB-231 cell line expressing OMD (231-Bo OMD) was similar to control cells
185 (231-Bo) (Figure S4F-I).

186 Based on the pattern of OMD staining in our cohort (Figure S2) and to determine which cells
187 in the tumour microenvironment were expressing OMD, we analysed available breast cancer
188 single cell RNAseq expression data including both stromal and epithelial cells[28]. We found that
189 CAFs but not other stromal cells consistently expressed OMD, and not epithelial cells as
190 previously hypothesized (Figure 3A-B). To further confirm OMD expression in the stroma, we
191 stained a tissue microarray of 482 breast cancer patient samples[29]. OMD staining was
192 detected only in stromal areas and not in tumour epithelium (Figure S5). The single cell
193 RNAseq and immunostaining analyses establish that OMD gene and protein are expressed
194 in CAFs. To validate this, we proceeded to collect CAF CM from our selected CAF cell line
195 544R. Using ELISA, we showed that CAF CM contained 45 ng/mL OMD while the 231-OMD
196 CM contained 96 ng/mL (Figure 3C). The CAF CM stimulated both 231-mA and MCF-7 cell
197 migration similarly to what we observed by adding rOMD (Figure 3D-G) and in line with
198 previous results (Figure 2). Overall, we established that OMD increases cell migration in ER+
199 and ER- breast cancer and is secreted in the tumour microenvironment by CAFs, suggesting
200 that fibroblasts play a role in inducing breast cancer metastasis to the bone.

201 **Phosphoproteomics Identifies an OMD-CDK1 Axis Driving Cell Migration and Viability**

202 To ascertain the mechanism underlying the role of OMD in breast cancer cell migration, we
203 analysed changes in the proteome and phosphoproteome of 231-OMD cells compared to 231-
204 mA (Figure 4, Figure S6). 231-Bo and 231-Bo OMD cells were used as further controls. We
205 identified and quantified 3971 proteins and 9423 phosphorylated sites (Tables S8-9). Pearson
206 correlation between biological replicates of the proteomic and phosphoproteomic data were
207 consistently over 0.97 and 0.6 respectively (Figure S6B-C). Across phosphorylated peptides,
208 41.9% were singly phosphorylated, 47.6% were doubly phosphorylated, and 10.5% were more
209 than doubly phosphorylated and the distribution of phosphorylated site residue across serine,
210 threonine and tyrosine was 85%, 11.3% and 3.7%, respectively, indicating enrichment on
211 tyrosine residues, with a median phosphorylated peptide score of 182 (Figure S6D-F). All the
212 quality controls were in line with previous publications [11,17]. Differential expression analysis
213 showed no differences between proteins expressed by 231-OMD and 231-mA ($P < 0.05$, Log2
214 Fold change > 1, Table S10) but identified 53 distinct phosphorylation sites, of which 18 were
215 upregulated and 35 were downregulated (Fig. 4A, Table S11). Of the 18 sites specifically
216 phosphorylated at higher levels in 231-OMD compared to 231-mA cells, only FOS like 1
217 (FOSL1) phosphorylation on serine 26 has a known cancer-associated function according to
218 Phosphosite plus [30] and has been shown to promote migration in MCF-7 breast cancer cells
219 [31]. Of the 35 downregulated phosphorylated sites in 231-OMD compared to 231-mA cells, 5
220 were also downregulated in 231-Bo OMD compared to 231-Bo cells, suggesting that these
221 sites are unlikely associated with the 231-OMD pro-migratory signalling mechanism and thus
222 they were excluded from further analysis (Table S11). Of the remaining 30 phosphorylated
223 sites specifically downregulated in 231-OMD compared to 231-mA cells, 6 had metastasis-
224 associated functions, such as promoting cell migration, invasion, or drug resistance according
225 to Phosphosite plus [30] (Figure 4A). Only one of these 30 downregulated sites was associated
226 with inactivation of protein activity which was Tyrosine 15 (Y15) on the cell cycle regulator,
227 Cyclin-dependent kinase 1 (CDK1, CDC2) [32] (Figure 4A, Table S11). We confirmed the
228 downregulation of Y15 on CDK1 in 231-OMD compared to 231-mA, 231-Bo OMD, and 231-
229 Bo cells by quantified immunoblotting (Figure 4B-C). Next, we searched for evidence of the

230 OMD-CDK1 crosstalk in available phosphoproteomics datasets analysing breast cancer
231 patient samples. We found an inverse relationship between OMD expression and reduction of
232 CDK1 inhibitory phosphorylation in two independent phosphoproteomics datasets analysing
233 105 and 122 breast cancer patients, respectively [11,33]. In these phosphoproteomics analyses,
234 CDK1 inhibitory phosphorylation at Y15 [32] was significantly reduced in patients where OMD
235 expression was above the mean compared to patients where OMD expression was below the
236 mean (Figure 4D-E). Therefore, the OMD-CDK1 axis may regulate the function of OMD.

237 To investigate the contribution of OMD and CDK1 to breast cancer metastasis, we analysed
238 2,765 breast cancer cases from KM Plotter[34]. We investigated high expression (n = 1697)
239 versus low expression (n = 1068) of both OMD and CDK1 using optimal cutoff over a follow-
240 up period of 180 months. The hazard ratio (HR) of high versus low expression was 1.63,
241 indicating a higher risk of recurrence in patients with high expression of OMD and CDK1
242 (Figure 4F). For ER+ patients, we investigated distant metastasis-free survival (DMFS) for
243 high versus low expression and revealed a hazard ratio (HR) of 1.81, demonstrating a higher
244 risk of relapse for patients with this subtype (Figure 4G). We further analysed the data to
245 ensure that OMD and CDK1 were independent prognostic factors (Table S12). In the analysis
246 of all tumors, the signature demonstrated independent prognostic value for DMFS, with a p
247 value of 0.045. In ER+ tumors, the signature showed strong prognostic performance, with a p
248 value of 1.1×10^{-4}. It surpassed all clinical parameters, including HER2 expression ($p = 0.055$),
249 lymph node status ($p = 0.104$), tumor grade ($p = 0.025$), tumor size ($p = 0.0002$), and patient
250 age ($p = 0.552$). These findings underscore the independent prognostic impact of the
251 signature, with its strongest predictive value observed in ER+ breast cancer cases (Figure
252 4G). Overall, the analysis found higher OMD/CDK1 to be a strong indicator of recurrence
253 independent of other prognostic variables, especially in ER+ patients, 20-40% of whom
254 experience metastasis and 70% of these correspond to bone.

255 **CDK1 Regulates Cell Migration and Viability *in vitro***

256 To verify the role of CDK1 downstream of OMD, we inhibited CDK1 using 10μM of the CDK1
257 inhibitor (CDK1i) RO-3306 [35] and assessed cell migration in the 231-mA and 231-OMD cells.
258 As expected, 231-OMD cells migrate more than 231-mA cells. However, only in 231-OMD was
259 cell migration significantly reduced upon treatment with 10μM RO-3306 (Figure 5A). To test
260 whether this reduction in migration was specifically downstream of CDK1, we inhibited CDK4/6
261 with 10μM of the clinically relevant inhibitor Palbociclib (CDK4/6i) and showed that its inhibition
262 did not significantly reduce 231-OMD cell migration (Figure 5A). Next, we investigated the
263 ability of CDK1 inhibition to block rOMD or CAF-derived CM in both ER+ and ER- cells. We
264 confirmed increased migration in response to rOMD which was effectively abrogated by RO-
265 3306 in both 231-mA and MCF-7 cells (Figs. 5B-C). The increased migration observed after
266 incubation with CAF-derived CM was also blocked by the CDK1i in both ER+ and ER- cell
267 lines (Figure 5D). Therefore, CDK1 is specifically activated in breast epithelial cells to regulate
268 cell migration *in vitro* and its inhibition decreases migration in response to OMD.

269 Given the known role of CDK1 in regulating cell cycle and cell viability [32], we studied the effect
270 of CDK1 inhibition on cell viability in both ER+ and ER- cells. We performed an Alamar blue
271 assay [36] on 231-mA, 231-OMD, and MCF-7 cell models and found that CDK1 inhibition only
272 reduced the viability of 231-OMD and MCF-7 cells treated with rOMD, but not 231-mA (Figs.
273 5E-F).

274 Finally, to test the clinical relevance of the OMD-CDK1 signalling axis, we used patient breast
275 cancer cells derived from metastatic pleural effusions and ascitic fluids (Figure 5G, Figure
276 S7A). Firstly, we assessed the effect of CDK1 activity on the viability of 5 metastatic patient-
277 derived breast cancers *in vitro*, of which 4 showed decreased cell viability in response to CDK1
278 inhibition (Figure S7B). Phosphoproteomics and proteomics analysis of these samples
279 produced a high-quality dataset (Figure S7C-G, Tables S13-14) and identified the
280 downregulation of Y15 on CDK1 in the 4 samples that responded to CDK1 inhibition and
281 reduced CDK1 Y15 phosphorylation significantly correlated with reduced viability in response
282 to 10μM RO-3306 treatment (Figure S7B, S7H, Table S14). Next, we studied 6 ER/PR positive

283 samples from ascites that had bone metastasis at the time of collection, 3 of which had
284 amplification of HER2 (Figure 5G). The ascitic fluid containing the breast cancer cells
285 expressed OMD at concentrations ranging from 30 to 1100 ng/mL (Figure 5H). We tested
286 CDK1 Y15 phosphorylation in the breast cancer cells derived from the ascitic fluid and
287 demonstrated low or no detectable phosphorylation, suggesting high activity of CDK1[37] (Figure
288 5I). We also assessed cell viability of these samples upon treatment with the CDK1 inhibitor
289 RO-3306 which demonstrated that 5 out of 6 samples responded (Figure 5J). The sample that
290 did not respond (BB3RC50) was the only sample where CDK1 Y15 phosphorylation was
291 evident by immunoblotting (Figure 5I). These data highlight the crucial role of active CDK1
292 downstream of OMD in regulating the viability of patient-derived breast cancer samples,
293 including those with bone metastases at the time of collection (Figure 5G).

294 Overall, these results indicate a mechanistic role for CDK1 downstream of OMD secreted from
295 fibroblasts in cellular processes relevant to metastasis such as cell migration and cell survival,
296 including in breast cancer cells derived from patients with bone metastases.

297 **OMD-CDK1 Axis Drives Bone Metastasis and Bone Colonization *in vivo***

298 Next, we assessed the effect of OMD on metastatic potential *in vivo*. To do this, we injected
299 231-mA, 231-OMD, and 231-BO (positive control for bone metastases) cells by intracardiac
300 injection into four athymic nude mice (Figure 6Ai). We found no significant differences in the
301 lung metastatic potential of 231-mA, 231-OMD, and 231-BO cells (Figure 6B). However, in
302 femoral bone flushes, the number of cytokeratin 19 (CK19)-positive cells, which is a marker
303 for human epithelial cells [27], was significantly higher in 231-OMD compared to 231-mA (Figure
304 6C-D). As expected, the bone-tropic 231-Bo also colonized the bone. This finding confirms a
305 role for OMD in the colonization of bone by breast cancer cells *in vivo*.

306 Since CDK1 regulates cell migration and viability in 231-OMD cells, we next tested whether
307 the OMD-CDK1 axis regulated bone colonization *in vivo.* To do this, we performed intracardiac
308 injection of 231-OMD cells into four athymic nude mice and tested whether inhibition of CDK1

309 affected the formation of bone metastasis (Figure 6Aii). We detected numerous CK19-positive
310 cells in bone flushes of mice treated with the vehicle control but almost no CK19-positive cells
311 in those treated with the CDK1 inhibitor RO-3306 (Figure 6E-F). Altogether, these *in vivo* data
312 indicate a role for the OMD-CDK1 axis in bone colonization by breast cancer cells.

313 In conclusion, we combined quantitative proteomics and phosphoproteomics from cancer
314 patients with bioinformatics analysis and functional assays *in vitro* and *in vivo* and showed that
315 OMD derived from CAFs regulates cell migration, cell viability and bone metastatic capabilities
316 through a CDK1-dependent mechanism.

317 Discussion

318 The yet unmet clinical need for novel biomarkers and targeted therapies to prevent and treat
319 breast cancer metastasis is demonstrated by the still very high number of deaths from breast
320 cancer each year of which 90% is caused by metastatic disease [2]. Here, we combined
321 quantitative proteomics and phosphoproteomics from breast cancer patient-derived samples
322 and cell models with bioinformatics analysis and functional assays *in vitro* and *in vivo*. We
323 demonstrated that OMD is expressed and secreted by cancer-associated fibroblasts (CAFs)
324 and stimulates the migration of ER-positive and ER-negative breast cancer cells. We found
325 that OMD requires the activation of CDK1 to regulate BC cell migration and cell viability and
326 to promote bone metastasis *in vivo*.

327 Our study establishes that proteomics and phosphoproteomics of patient samples with known
328 outcome at 5 years will identify novel drivers of metastasis. This time period was selected
329 based on the available clinical outcome data. The aim was to derive proteins that could be
330 used as biomarkers or drug targets in the clinic, as dysregulated genes or RNA transcripts
331 identified in patient samples poorly correlate with the proteomics changes seen in metastases
332 [8,33]. Among the limitations of proteomics analysis of large cohort of patient samples are the
333 availability of fresh frozen rather than paraffin-embedded (not yet suitable for
334 phosphoproteomics) matched primary and metastatic samples and of the clinical information

335 associated with them. Our proteomics and phosphoproteomics analysis of fresh frozen
336 primary breast cancer resection samples provides therefore a unique resource as samples
337 were manually annotated to determine the presence or absence of organ-specific metastases
338 within five years of diagnosis [38,39]. More recent approaches, including spatial proteomics[40] and
339 single-cell proteomics[41] analysis of large cohort of clinical samples, will enable further
340 discoveries in the near future.

341 Our proteomics analysis identified OMD, a monomeric member of the small leucine-rich repeat
342 protein (SLRP) family [42], as significantly upregulated in patients who developed bone
343 metastases compared to those who developed metastases at other metastatic sites or who
344 did not develop metastases. The transcript of OMD was previously identified as enriched in
345 breast cancer bone metastases compared to breast cancer metastases in other organs [10] and
346 in prostate cancer bone metastases [19]. These findings suggest that OMD may be a pan-cancer
347 biomarker for bone metastases. OMD regulates important cancer pathways, including Ras,
348 P53, Jun/Fos, MYC, and NFκB signalling [24] but little is known about its role in cancer
349 phenotypes. Although our data exclude a primary role for OMD in the tested functions of
350 fibroblasts and osteoclasts using available cell models, OMD may play a role in promoting
351 bone turnover, which is an essential step in osteosclerotic bone metastases [25]. OMD is known
352 to reduce apoptosis in osteoblasts [43], thus supporting a role for OMD in promoting new bone
353 formation and cell survival. Indeed, in our patient cohort upregulated OMD expression
354 correlates with upregulation of serine 118 phosphorylation on pro-apoptotic protein BCL2-
355 associated agonist of cell death (BAD) (Table S5). This site prevents BAD interaction with
356 BCL2 Like 1, thus preventing apoptosis [44]. We establish here that OMD regulates cell
357 migration in both ER+ and ER- cell lines and that secretion of OMD is from CAFs, not tumour
358 cells. We validate this by showing that CAFs secrete biologically relevant concentrations of
359 OMD[45], which stimulate tumour cell migration. In support of this mechanism, recent data
360 demonstrate cancer-associated fibroblasts are strongly associated with bone metastasis in
361 over 300 early invasive ductal breast cancer patients [46].

362 Secreted OMD [24] engages cell surface receptors, such as the BMP2 receptor complex [45], and
363 integrin $\alpha_V\beta_3$, both of which are associated with bone metastasis [47,48]. In support of this idea,
364 we identified BMP2-induced kinase (BMP2K) and FAK activity downstream of OMD (Table
365 S11 and data not shown). Crosslinking[49] and cell-surface capture mass spectrometry[50], or
366 functional kinase profiling assays could be used to identify other candidates and elucidate the
367 signalling pathways downstream of OMD in breast and other cancer cells. Phosphoproteomics
368 analysis identified a correlation between elevated OMD expression and increased activation
369 of the kinase CDK1 in both cell models and patient samples. Therefore, OMD expression may
370 inform clinicians as to which patients could benefit from CDK1 inhibition. Indeed, we
371 demonstrated the independent prognostic impact of a OMD/CDK1 signature on metastatic
372 recurrence in over 2,600 breast cancer patients, with the strongest predictive value observed
373 in ER+ cases. This would require further validation at the protein level to develop an effective
374 biomarker to select for OMD/CDK1 therapy to prevent bone metastasis.

375 Osteoblasts express and secrete OMD[51,52], and it is therefore feasible that when cancer cells
376 arrive in the bone microenvironment, osteoblast-secreted OMD enables cancer cell
377 colonisation. Furthermore, CDK1 phosphorylates and activates RUNX2, which can induce a
378 variety of bone-related genes [53,54], and we speculate that OMD may drive bone metastasis
379 through CDK1-RUNX2 [55,56].

380 We validated that the OMD-CDK1 axis is a driver of cell viability and motility, consistent with
381 the role of CDK1 not only in cell cycle regulation, but also in actin remodelling, a key process
382 in cell migration [57]. We also found increased phosphorylation of vimentin on Serine 56 (Table
383 S5), which regulates cancer cell invasion [58], in patients who developed metastases compared
384 to those who did not (Table S5). The intriguing role of CDK1 as a driver of cell migration and
385 potential metastasis deserves further investigation in breast and other cancers. Indeed, CDK1
386 mRNA is upregulated not only in several transcriptomics datasets of breast cancer samples
387 compared to normal breast tissue samples [59], but also in melanoma [60], thyroid cancer [61] and
388 acute myeloid leukaemia [20]. Additionally, our study investigating tumour cells derived from

389 patients with bone metastases showed a relationship between OMD protein expression, CDK1
390 activation (reduced Y15 phosphorylation) and reduced cell viability in response to CDK1
391 inhibitor. As discussed above, OMD may activate BAD to drive the survival of breast cancer
392 patient cells during bone metastasis. Finally, we demonstrate higher bone colonisation after
393 intracardiac injection of OMD-overexpressing tumour cells and that this can be abrogated by
394 treatment with a CDK1 inhibitor. Overall, our data suggest that CDK inhibition could serve as
395 a novel therapeutic route to decrease motility, viability and bone metastasis in breast cancer.
396 However, the CDK1 inhibitor RO-3306 has been used in few studies *in vivo* [62,63] and no CDK1-
397 selective inhibitor has been tested in clinical trials in breast or other cancers [64]. Future studies
398 should aim at testing other CDK1-selective inhibitors or CDK1 inhibition in combination with
399 other signalling inhibitors. For instance, among the phosphorylated sites significantly
400 upregulated in patients who developed metastases compared to those who did not, we also
401 found phosphorylated ser 641 on catenin alpha 1 (CTNNA1) (Table S5) which activates beta
402 catenin signalling resulting in tumour cell invasion [65] and phosphorylated Thr185/Tyr187 on
403 MAPK1 which are hyperactive in metastatic TNBC [13] (Table S5). Therefore, our data provides
404 the rationale for the targeting of MAPK and beta catenin signalling pathways in combination
405 with or independently of CDK1 inhibition to prevent metastasis.

406 In conclusion, the identification of the OMD-CDK1 axis from patient-derived samples with
407 complete clinical information suggests that similar studies can be performed in any cancer
408 setting including across multiple cancers to identify novel biomarkers, organotropic metastatic
409 drivers, and therapeutic targets. Here, OMD was discovered to be significantly upregulated in
410 primary breast cancer biopsies of patients who developed bone metastases within five years
411 of diagnosis, compared to those who were distant disease free at 5 years. OMD significantly
412 increased cell migration and cell viability as well as bone colonisation of breast cancer cells
413 and of breast cancer cells derived from patients with bone metastases. Migration, viability and
414 bone colonisation induced by CAF-derived OMD were CDK1-dependent and thus highlight a

key tumour-stroma interaction in bone metastasis establishing the OMD–CDK1 axis as a potential therapeutic target in metastatic breast cancer.

Resource Availability

Data and code availability

All raw MS data were generated by the authors and deposited to the ProteomeXchange Consortium, via the PRIDE partner repository with the dataset identifier PXD041719 (Username: reviewer_pxd041719@ebi.ac.uk; Password: 4PS3MTqM); PXD041720 (Username: reviewer_pxd041720@ebi.ac.uk; Password: Tr6QtMFt); PXD042764 (Username: reviewer_pxd042764@ebi.ac.uk; Password: rsDlM5NX).
The R scripts related to this publication are freely accessible at https://github.com/Joseph-Parsons/OMD/.

Acknowledgments

Funding: This work was supported by Engineering and Physical Sciences Research Council grant EP/S022201/1 (SC), CR-UK Non-Clinical Training Award A27445 (JP), Medical Research Council grant MR/T016043/1 (PF, DB, JF, MPS, JW), Breast Cancer Now (HH, KS, PO, DL), Stanley Center for Psychiatric Research at Broad Institute (KT), NIHR Manchester Biomedical Research Centre (TK, NA), Cancer Research UK Manchester Institute Histology Core Facility (CB), Yorkshire Cancer Research, Western Park Cancer Charity (PO), National Institute for Health Research (COB), Cancer Research UK, National Institute for Health Research, UK Research and Innovation, Breast Cancer Now (RBC), Wellcome Trust 107636/Z/15/Z and 107636/Z/15/A, the Biotechnology and Biological Sciences Research Council BB/X001970/1 and Medical Research Council MR/T016043/1, the NNF Young Investigator Award call 2022, NNF22OC0070845 (CF). For the purpose of open access, the author has

applied a CC BY public copyright licence to any Author Accepted Manuscript version arising from this submission.

We thank the CRUK Manchester Institute Histology and Visualisation, Imaging and Analysis facilities for their support with immunohistochemical optimisation and visualisation, the University of Manchester Bio-MS, Genome Editing, and Imaging facilities for their continuing support throughout the project. We thank Dr Hurlstone, University of Manchester for providing invaluable reagents and protocols.

Author contributions. S.C., J.P. performed the research and interpreted data. H.H., T.K., P.F., K.S., D.B., J.F., J.F., C.B., N.A., M.P.S, P.O., D.L., J.B. contributed to the research and interpreted data. J.W., K.T., M.J.D., B.G. supported and contributed to the bioinformatic analyses. C.O.B. devised and supervised the project and collated information on patient samples for mass spectrometry-based analysis. CF devised and supervised the project, designed mass spectrometry and *in vitro* experiments, and obtained funding for the project. RBC devised and supervised the project, designed *in vitro* and *in vivo* experiments, and obtained funding for the project. All authors reviewed and approved the manuscript before submission.

Declaration of interests

The authors declare no potential conflicts of interest. All authors give consent for publication.

460 **STAR Methods**

461 **Key Resources Table**

Consumables	
Covaris microtube-500 AFA Fiber Screw Cap (520185)	Covaris
Sep-Pak Classic C18 Cartridges (WAT051910)	Waters
Solid Phase Extraction Disk “EMPORE” C18 3M (2315)	Agilent Technologies
Solid Phase Extraction Disk “EMPORE” C8 3M (2314)	Agilent Technologies
Cells	
MDA-MB-231 Parental Cells	Gift from Joan Massagué[27,66]
MDA-MB-231 Bone-Tropic Cells	Gift from Joan Massagué[27,66]
MCF-7	ATCC
HMFU19 Immortalised Normal Fibroblasts	Gift from Cliona Kirwan[67]
544R Immortalised Cancer-Associated Fibroblasts	Gift from Cliona Kirwan[68]
HFOB 1.19 (CRL-11372)	ATCC
RAW 264.7 Mouse Monocytes	Gift from Penny Ottewell[69]
Lenti-X 293T	Gift from Adam Hurlstone[70]

XL1 Blue *E.coli* (200249)	Agilent
Kits	
ReliaPrep™ RNA Cell MiniPrep System (Z6011)	Promega
GoScript™ Reverse Transcription System (A5001)	Promega
Click-iT™ EdU Cell Proliferation Kit for Imaging, Alexa Fluor™ 488 dye (C10337)	ThermoFisher
Alkaline Phosphatase Assay Kit (ab83368)	Abcam
VenorGem Classic Mycoplasma Detection Kit (11-1025)	Minerva Biolabs
QIAquick Gel Extraction Kit (28706X4)	Qiagen
QIAPrep Spin Miniprep Kit (27106X4)	Qiagen
Human Osteoadherin/Osteomodulin PharmaGenie ELISA Kit (SBRS0954)	AssayGenie
Pierce™ BCA Protein Assay Kit (23225)	ThermoFisher
Reagents	
Bicinchoninic Acid Solution (B9643-1L)	Merck
Copper (II) Sulfate Solution (C2284)	Merck
Trypsin Porcine Pancreas (T6567)	Sigma-Aldrich

Lysyl Endopeptidase/Endopeptidase C (12505061)	Fujifilm
Trifluoroacetic Acid (76-05-1)	Sigma-Aldrich
Acetonitrile (75-05-8)	Merck
Titanium Dioxide Beads “Titanspheres” (5020-75000)	GL Sciences
Formic Acid (64-18-6)	Merck
Stable Cell DMEM (0819)	Sigma-Aldrich
RPMI (R0883)	Sigma-Aldrich
DMEM-F12 (31330-038)	Gibco
DMEM-F12 no phenol red (21041025)	Gibco
Advanced DMEM/F12 (12634)	Gibco
B27 Supplement (12587-010)	Gibco
Epidermal Growth Factor (E9644)	Sigma-Aldrich
Hydrocortisone (H0888)	Merck
L-Glutamine (25030081)	ThermoFisher
Poly(2-hydroxyethyl methacrylate)/polyHEMA (P3932)	Merck
Phosphate Buffered Saline 1X (D8662)	Sigma-Aldrich
Trypsin-EDTA 0.05% (T3924)	Sigma-Aldrich

Penicillin-Streptomycin (P0781)	Sigma-Aldrich
Sodium Pyruvate (S8636)	Sigma-Aldrich
Foetal Calf Serum Qualified (10270106)	Gibco
Recombinant Human RANKL (390-TN)	Biotechne (RND Systems)
Recombinant Human OMD (10825-H08H)	SinoBiological
FuGENE HD Transfection Reagent (E2311)	Promega
VSV-G Envelope expressing plasmid pMD2.G	Gift from Adam Hurlstone[70]
pMDLg/pRRE Lentiviral Packaging Plasmid	Gift from Adam Hurlstone[70]
pRSV-Rev Lentiviral Packaging Plasmid	Gift from Adam Hurlstone[70]
NotI Restriction Enzyme (R3189S)	New England Biolabs
NheI Restriction Enzyme (R3131S)	New England Biolabs
CIP (Calf Intestinal Alkaline Phosphatase) (M0290S)	New England Biolabs
T4 Ligase (M0202S)	New England Biolabs
qPCRBIO SyGreen Mix (PB20.14-05)	PCR Biosystems
Clarity Western ECL Substrate (1705061)	Bio-rad
Mitomycin (10022604)	Fisher Scientific
RO-3306 (217699)	Sigma-Aldrich
Palbociclib (S1116)	Selleck

Haemotoxylin (6765008)	Epredia
Eosin Y Alcoholic (6766008)	Epredia
Neutral Buffered Formalin 4%	Genta Medical
Triton x-100 (X100)	Sigma-Aldrich
Dako pH9 Antigen Retrieval Solution (S2367)	DAKO
Hydrogen Peroxide 30% solution (H1009)	Sigma-Aldrich
Casein 10X (SP5020)	Vector Labs
Mouse-on-Mouse Detection Kit (MP2400)	Vector Labs
ARK (Animal Research Kit) (K3954)	DAKO
Avidin/Biotin Blocking Kit (SP2001)	Vector Labs
Hoechst 3342 (4082S)	New England Biolabs
Bovine Serum Albumin (A30075)	Melford
PureCol Type I Bovine Collagen Solution (5005)	Advanced Biomatrix
Matrigel (354234)	Corning
Crystal Violet (C0775)	Sigma-Aldrich
Alizarin Red (A5533)	Sigma-Aldrich
Toluidine Blue (T3260)	Sigma-Aldrich
0.4mm Bovine Cortical Bone Slices	Boneslices.com

Alamar Blue Reagent (DAL1025)	ThermoFisher
Antibodies Antibodies were diluted 1:1000 for immunoblotting and 1:100 for immunohistochemistry except Vinculin and GAPDH loading controls which were using in immunoblotting at 1:10000 and OMD for immunohistochemistry which was used at 1:50. Antibodies were validated for the species and application on the manufacturer's websites.	
Anti-Phospho-Tyrosine Mouse Antibody – Sepharose Bead Conjugate (9419)	Cell Signalling
PTMScan(R) Tyr Motif IAP Beads (1991S)	Cell Signalling
PTMScan Phospho-tyrosine Rabbit Antibody (P-Tyr-1000) (8803)	Cell Signalling
Anti-Osteomodulin Polyclonal Rabbit Antibody (NBP2-19626)	Novus Biologicals
Anti-Vinculin Mouse Monoclonal Antibody (V9624)	Sigma-Aldrich
Anti-T2A Mouse Monoclonal Anitbody (NBP2-59627)	Novus Biologicals
Anti-Cytokeratin 19 Antibody (MO888)	DAKO
Anti-cytokeratin 19 antibody (M8888) used in Fig 5C-D	Agilent
Anti-phosphorylated CDK1 (Y15) Rabbit Polyclonal Antibody (A14600)	Abclonal

Anti-CDK1 Rabbit Polyclonal Antibody (131450)	Abcam
Vectors	
pCDH1-Ef1-MCS-T2A-mApple vector	University of Manchester[70]
Primers	
Beta Actin: Fwd TGGAACGGTGAAGGTGACAG Rev AACAACGCATCTCATATTTGGAA	In-house
RANKL: Fwd CAACATATCGTTGGATCACAGCA Rev GACAGACTCACTTTATGGGAACC	In-house
IBSP: Fwd CACTGGAGCCAATGCAGAAGA Rev TGGTGGGGTTGTAGGTTCAAA	In-house
SPARC: Fwd TGAGGTATCTGTGGGAGCTAATC Rev CCTTGCCGTGTTTGCAGTG	In-house
CDH11: Fwd AGAGAGCCCATACACGTTGA Rev TTGGCATGATAGGTCTCGTGC	In-house
Mouse Beta Actin: Fwd GGCTGTATTCCCCTCCAT Rev CCAGTTGGTAACAATGCCATGT	In-house

Mouse CTSK: Fwd AATACCTCCCTCTCGATCCTACA Rev TGGTTGTTGACTGGAGTAACGTA	In-house
Mouse OSCAR: Fwd CCGTGCTGACTTCACACCAA Rev GGGGTGACAAGGCCACTTTT	In-house
Software	
MaxQuant version 1.5.6.5	[71]
Perseus version 1.6.10.45	[72]
STRING version 11.5	[73]
Cytoscape version 3.4.0	[74]
R Framework version 4.2.1	http://www.rstudio.com/
RStudio version 2022.02.3	http://www.rstudio.com/
OlyVIA	Olympus LifeScience
ImageJ version 1.52	[75]
SkanIt version 6.1	ThermoFisher
QuPath version 0.2.3	[76]

462

463 **Ethics approval**

464 Early breast cancer samples were collected from patients undergoing surgical resection of the
465 primary tumour at the Manchester University NHS Foundation Trust through the Manchester

466 Cancer Research Centre Biobank. Metastatic fluids (ascites or pleural effusions) drained from
467 advanced breast cancer patients were collected at the Christie and South Manchester
468 Hospitals NHS Foundation Trusts through the Manchester Cancer Research Centre Biobank.
469 Fully informed consent from all patients was obtained in accordance with local National
470 Research Ethics Service guidelines (study numbers: 05/ Q1402/25, 05/Q1403/159, and
471 12/ROCL/01). Patient samples from the University of Sheffield sponsored AZURE trial
472 were obtained with fully informed patient consent. AZURE was approved by the Clinical Trials
473 Committee; controlled trials number ISRCTN79831382[29].

474 ***In vivo* Experiments**

475 All *in vivo* experiments were performed in accordance with the Animals (Scientific Procedures)
476 Act 1986 under the UK Home Office project licence PCFEAC0D4 and study protocols were
477 approved by the CRUK Manchester Institute Animal Welfare and Ethical Research Board
478 (AWERB). 100,000 PAM, PAO, or BOM cells in 50µl PBS were injected into the left cardiac
479 ventricle of 4 athymic nude mice (sourced from Envigo) per condition using a 28-gauge needle.
480 Mice were monitored for 25 days before culling. For CDK1 inhibition studies, 4 days after
481 intracardiac injection of 100,000 PAO cells, 4 athymic nude mice were dosed with 225µl of
482 RO-3306 solution (final concentration 4mg/kg, SeleckChem) dissolved in 40% PEG300-1%
483 Tween80-3% DMSO in ddH_2O given 3 times per week by oral gavage and compared to 4
484 vehicle control mice. Mice were culled 25 days after intracardiac injection of breast cancer
485 cells. Lungs (only for the first study) and one femur were formalin-fixed for
486 immunohistochemical analysis, and one femur was collected in DMEM with FCS, 10% Pen-
487 Strep and 1mM Sodium pyruvate and bones were flushed. To flush bones, the ends of mouse
488 femurs were clipped using scissors and ground down and the bone marrow was flushed using
489 5mL complete DMEM using a 25-gauge needle. The ground bone ends and bone marrow
490 were filtered through a 100µm filter which was washed with 5mL complete DMEM. Filtered
491 bone cells were pelleted by centrifugation at 600xg at 4°C before filtering through a 40µm
492 filter.

493 **Sample Preparation for Proteomics and Phosphoproteomics**

494 Fresh frozen primary breast cancer patient samples were ground using a pestle and a mortar
495 filled with liquid nitrogen to prevent tissue thawing. Technical replicates of 9 samples were
496 used to assess reproducibility of the method. For both fresh frozen primary breast cancer
497 patient samples and metastatic effusion samples, 6M guanidine hydrochloride in 100mM Tris
498 pH 8.5 at 99ºC was immediately added to the ground tissue and samples were heated at 99
499 degrees for 10 minutes in an Eppendorf shaker at 600rpm. Lysates were transferred to Covaris
500 sonicator tubes and sonicated in a Covaris E220 (Covaris) three times for three minutes cycles
501 with peak power of 500, duty factor 30%, 200 cycles/burst and 150 average power. Protein
502 concentration was assessed using bicinchoninic acid assay (ThermoFisher). 750ug of protein
503 was digested to peptides using Endopeptidase C for 1 hour before dilution with 25mM Tris pH
504 8.5 and further digestion with trypsin overnight. Trifluoroacetic acid (TFA) was added to 1%
505 concentration to eliminate further trypsin activity. Samples were desalted using SepPak
506 columns (Waters), eluted using 50% acetonitrile (ACN) dried using an Eppendorf
507 Concentrator, resuspended in 10mM ammonium hydroxide (NH_4OH) pH 10 and fractionated
508 using a StageTip-based reverse phase fractionation method. StageTips were initially activated
509 with methanol, 5mM NH_4OH 50% ACN and 10mM NH_4OH before loading samples, taking a
510 flow-through fraction, and subsequently eluting with 1% ACN and 7% ACN into different
511 fractions. A 50% ACN fraction is taken to remove any remaining peptides bound to the C18
512 disks. The same fractionation with a flow-through, 1%, 7% and 50% ACN fraction was
513 performed on a second tip. The flow through and 50% fractions were combined, both 1%
514 fractions were combined and both 7% fractions were combined. 5% of each sample was
515 retained for proteome analysis. The remaining 95% was acidified with 6% TFA in 50% ACN
516 before incubation with titanium dioxide coated beads (GL Sciences) in 20mg/ml
517 dihydroxybenzoic acid (DHB) resuspended in 80% ACN, 6% TFA and deionised water, as
518 previously described[17]. Beads were centrifuged onto a C8 disc (EMPORE) and then were
519 washed with 10% ACN 6% TFA followed by 40% ACN 6% TFA and 80% ACN 6% TFA before

520 subsequently being eluted using 5% ammonia and 10% ammonia in 25% ACN. Both proteome
521 and phosphoproteome samples were loaded onto C18 StageTips (EMPORE) for an additional
522 desalting step before elution using 40% ACN. Samples were then reduced to 5ul using an
523 Eppendorf Concentrator and resuspended in 25ul 0.1% Formic Acid, 5% TFA before analysis
524 on the mass spectrometer.

525 MDA-MB-231 cells (three independent biological replicates of 231-mA, 231-OMD, 231-Bo and
526 231-Bo OMD) were lysed with 6M GuHCl in 100mM Tris pH 8.5 heated to 99°C. Lysates were
527 sonicated and protein concentration assessed as above. 1.5mg of protein per sample was
528 digested and desalted as above. Dried samples were resuspended in 50mM MOPS pH 7.2,
529 10mM Sodium Phosphate, 50mM Sodium Chloride (NaCl) and dissolved overnight. Samples
530 were clarified by centrifugation and clarified peptides were incubated in a new tube with
531 immobilised phosphorylated tyrosine antibody beads (Cell Signalling) and incubated for 2
532 hours at 4°C. Beads were washed five times with the MOPS buffer and twice with 50mM NaCl.
533 Phosphorylated tyrosine-enriched peptides were eluted from the beads three times using
534 0.1% TFA. Unbound samples were processed as above with 5% of sample retained for
535 proteome analysis and the rest being used for phosphorylated peptide enrichment. Proteome,
536 phosphoproteome and phosphorylated tyrosine-enriched samples were loaded onto C18
537 StageTips, eluted using 40% ACN, reduced to 5ul and resuspended in 0.1% Formic acid, 5%
538 TFA before analysis on the mass spectrometer.

539 Cells from metastatic effusions were pelleted by centrifugation, the supernatant was removed,
540 and cells were lysed and processed for proteomic analysis via the same processes as
541 MDAMB231 cell lines, described above.

542 **Mass Spectrometry Analysis**

543 Mass spectrometry analysis was performed as described[17]. Briefly, purified peptides were
544 analysed by LC-MS/MS using an UltiMate 3000 Rapid Separation LC (ThermoFisher) coupled
545 to an Orbitrap Exploris 480 mass spectrometer (ThermoFisher). Mobile phase A was 0.1% FA

546 in water, and mobile phase B was 0.1% FA in ACN and the column was a 75 mm x 250 µm
547 inner diameter 1.7 µM CSH C18, analytical column (Waters). A 1 µl aliquot of the sample (for
548 proteome analysis) or a 3 µl aliquot was transferred to a 5 µl loop and loaded on to the column
549 at a flow of 300 nl/min at 5% B for 5 and 13 min, respectively. The loop was then taken out of
550 line and the flow was reduced from 300 nl/min to 200nl/min in 1 min., and to 7% B. Peptides
551 were separated using a gradient that went from 7% to 18% B in 64 min., then from 18% to
552 27% B in 8 min. and finally from 27% B to 60% B in 1 min. The column was washed at 60% B
553 for 3 min. and then re-equilibrated for a further 6.5 min. At 85 min, the flow was increased to
554 300nl/min until the end of the run at 90min. Mass spectrometry data were acquired in a data-
555 dependent manner for 90 min in positive mode. Peptides were selected for fragmentation
556 automatically by data-dependent analysis on a basis of the top 8 (phosphoproteome analysis)
557 or top 12 (proteome analysis) with m/z between 300 and 1750Th and a charge state of 2, 3 or
558 4 with a dynamic exclusion set at 15 s. The MS resolution was set at 120,000 with an AGC
559 target of 3e6 and a maximum fill time set at 20ms. The MS2 resolution was set to 60,000, with
560 an AGC target of 2e5, and a maximum fill time of 110 ms for Top12 methods, and 30,000, with
561 an AGC target of 2e5, and a maximum fill time of 45 ms for Top8 analysis. The isolation
562 window was of 1.3Th and the collision energy was set at 28.

563 **Data Analysis**

564 Raw files were analysed by the MaxQuant software suite[71] (version 1.5.6.5) using the
565 integrated Andromeda search engine. Proteins were identified by searching the HCD-MS/MS
566 peak lists against a target/decoy version of the human UniProt Knowledgebase database that
567 consisted of the complete proteome sets and isoforms (v.2019;
568 https://uniprot.org/proteomes/UP000005640_9606) supplemented with commonly observed
569 contaminants such as porcine trypsin and bovine serum proteins. Tandem mass spectra were
570 initially matched with a mass tolerance of 7 ppm on precursor masses and 0.02 Da or 20 ppm
571 for fragment ions. Cysteine carbamidomethylation was searched as a fixed modification.
572 Protein N-acetylation, N-pyro-glutamine, oxidized methionine and phosphorylation of serine,

573 threonine and tyrosine were searched as variable modifications. Protein N-acetylation,
574 oxidized methionine and deamidation of asparagine and glutamine were searched as variable
575 modifications for the proteome experiments. Label-free parameters were used. False
576 discovery rate was set to 0.01 for peptides, proteins, and modification sites. Minimal peptide
577 length was six amino acids. Site localization probabilities were calculated by MaxQuant using
578 the PTM scoring algorithm. The datasets were filtered by posterior error probability to achieve
579 a false discovery rate below 1% for peptides, proteins, and modification sites. Only peptides
580 with Andromeda score > 40 were included in the downstream analysis.

581 For patient sample analysis, proteome quality control included proteins with more than 2
582 razor+unique peptides and greater than 5% protein sequence coverage. For the
583 phosphoproteome, localisation probability of 0.7 or higher was required for each site. Samples
584 with fewer than 2000 proteins or 2000 phosphorylated sites were excluded. Only proteins and
585 sites that were present in at least 80% of either non-metastatic or metastatic samples were
586 included in the final analysis. For cell line and metastatic effusion samples, we used the same
587 criteria as above and we included only proteins or phosphorylated sites that were present in
588 all samples.

589 All statistical and bioinformatics analysis was done using freely available software and
590 packages: Rstudio (R version 4.2.1, Rstudio version 2022.02.3) (http://www.rstudio.com),
591 Perseus (version 1.6.10.45)[72], STRING (version 11.5)[73], and Cytoscape (version 3.4.0)[74].
592 Differential expression analysis performed separately on proteome and phosphoproteome
593 using Rstudio package DEP (Bioconductor version 3.15). All peptide intensities were
594 normalised using the normalizeQuantiles function in the R package Limma[77]. Normalised
595 peptides were subjected to left-centred imputation and differential expression analysis using
596 the R packages DEP (PMID: 29446774) and Limma[77]. Differentially expressed proteins or
597 phosphorylated sites were defined in patient samples as those with a p value of less than 0.05
598 and a Log2 fold change of less than -1.5 or greater than +1.5, and in cell lines as those with a
599 p value of less than 0.05 and a Log2 fold change of less than -1 or greater than +1. Hierarchical

600 clustering and Vulcano plots analyses were performed using Perseus. Protein-protein
601 interactions networks were generated using STRING. Data were visualised with Cytoscape.

602 **Analysis of the GEO datasets and single cell RNA seq dataset**

603 The analysis of OMD expression in GEO datasets shown in Fig. 1F was performed using
604 Table 2 from reference[10]. Single cell RNA seq dataset was analysed using the online platform
605 CELLxGENE[28].

606 **Generation of a Database of Breast Cancer Metastasis-Associated Genes and Proteins**

607 This database was generated using the PubMed search term "Breast Cancer Metastasis" and
608 collecting the first 300 most relevant texts. Genes and proteins dysregulated in breast cancer
609 metastasis were extracted from papers and presented in the database with gene name,
610 protein name(s), a short summary of their contribution to breast cancer metastasis, the
611 reference for the energy, any specific organotropism associated with the entry and the level
612 at which the dysregulation occurs e.g., genomics, transcriptomic or proteomic.

613 **Kaplan-Meier analysis**

614 Gene IDs for OMD (205907_s_at, 205908_s_at) and CDK1 (203214_x_at, 210559_s_at,
615 203422_at, 203213_at) were used as input to the breast cancer mRNA gene chip dataset at
616 kmplot.com[34] to evaluate the effects of the two-gene signature on distant metastasis-free
617 survival. All patients and patients with estrogen receptor positive subtype were dichotomized
618 according to the auto selected best cutoff percentile of the mean expression of the gene
619 signature and the threshold set at 180 months.

620 **Multivariate Survival Analysis**

621 To assess the prognostic significance of a two-gene signature in breast cancer, we performed
622 a comprehensive search in the GEO (https://www.ncbi.nlm.nih.gov/geo/) and EGA
623 (https://ega-archive.org/) repositories. Transcriptomic datasets with DMFS data, with a

624 minimum of 30 samples, were included and focused on those generated using the platforms
625 GPL96, GPL570, and GPL571. The datasets used in this analysis were GSE2990, GSE3494,
626 GSE6532, GSE7390, GSE11121, GSE5327, GSE9195, GSE16446, GSE17907, GSE19615,
627 GSE20685, GSE26971, GSE16716, E-TABM-43, GSE45255, GSE25066, GSE22093,
628 GSE65194, GSE69031, GSE58812, and GSE61304. This selection ensured the use of a
629 consistent set of 22,277 genes across datasets, allowing for uniform sensitivity, specificity,
630 and dynamic range. Each dataset underwent rigorous normalization and quality control.
631 Initially, normalization was conducted using MAS5, a method chosen for its superior
632 performance in previous comparisons with RT-PCR-validated expression data. MAS5 also
633 enables the normalization of individual samples independently, which prevents the
634 recalibration of values when adding or removing samples. To reduce batch effects, a second
635 normalization step was applied, scaling the mean expression of overlapping probes to a value
636 of 1,000 across all arrays. Redundant samples with identical gene expression profiles were
637 identified and excluded, retaining only the earliest version to ensure unique biological
638 representation. Quality control metrics were assessed across five parameters, including
639 background signal, raw Q values, the percentage of present calls, bioBCD spike-in controls,
640 and the GAPDH/ACTB 3-to-5 ratio. Samples were deemed acceptable if they met the
641 expected range for all parameters, while outliers and biased arrays, failing two or more criteria,
642 were excluded from downstream analyses. Following this process, 2,828 unique samples with
643 high-quality data were retained for subsequent analysis. The two-gene signature was
644 constructed by calculating the mean expression of the probes corresponding to OMD
645 (osteoadherin) and CDK1 (cyclin-dependent kinase 1). The signature utilized six probe sets:
646 205908_s_at, 205907_s_at (OMD), and 203214_x_at, 210559_s_at, 203422_at, 203213_at
647 (CDK1). Survival analysis was performed to evaluate the association between the signature
648 and distant metastasis-free survival (DMFS). The mean expression of the signature was
649 assessed across potential cutoff values spanning the interquartile range, with statistical
650 significance determined using Cox proportional hazards regression models. False Discovery
651 Rate (FDR) correction was applied using the Benjamini-Hochberg method. Subgroup

652 analyses were conducted for estrogen receptor-positive (ER+), triple-negative breast cancer
653 (TNBC), and all tumors collectively. The independent prognostic value of the signature was
654 further assessed using multivariate Cox regression, accounting for available clinical and
655 pathological parameters including HER2 expression, lymph node status, tumor grade, tumor
656 size, and patient age.

657 **Immunohistochemistry**

658 500,000 bone marrow cells were pelleted onto glass slides using a Shandon Cytospin 3
659 centrifuge at 600rpm. Cytospin samples were fixed in 4% neutral-buffered formalin in PBS and
660 permeabilised with 0.25% Triton X-100. Endogenous peroxidases were blocked with hydrogen
661 peroxide (10%), samples were blocked with Casein. Samples were incubated with 200µg/ml
662 anti-Cytokeratin 19 primary antibody (CK19) was biotinylated using DAKO Animal Research
663 kit (ARK) and incubated on samples for 30 minutes at room temperature. ARK kit anti-biotin
664 secondary antibodies were incubated on samples for 30 minutes before staining with DAB
665 stain to produce a colorimetric response. Gills I haemotoxylin was used for counterstaining
666 and samples were coverslipped before imaging. TBST washes were performed between each
667 step. Whole slide imaging was performed using Olympus VS200 MTL (Olympus Life Science)
668 in conjunction with an Olympus UPLXAPO20X objective lens and 20x magnification. Lung
669 metastatic tumour lesions, identified in collaboration with Visualisation, Imaging and Analysis
670 Core Facility at Cancer Research UK Manchester Institute, of greater than 100µm in diameter
671 (in one orientation) were counted using OlyVIA to assess the number of macrometastases in
672 the lungs. For quantification of cytokeratin 19-positive cells in cytospins of the bone marrow
673 flushes for figure 6C and D, slides were scanned and images were opened in OlyVIA and
674 sample coordinates were determined and a random number generator was used to select
675 coordinates in which five fields of view at 10X magnification were used to count the number of
676 CK19-positive cells. For quantification of cytokeratin 19-positive cells in cytospins of the bone
677 marrow flushes for figure 6E and 6F, slides were scanned, and images were opened in OlyVIA
678 and all 4 quadrants of the cytospins were scored to enumerate the CK-positive cells in control

679 and CDK1 inhibitor treated mice. Immunohistochemical staining of patient samples for
680 osteomodulin required sample dewaxing in xylene, washing sequentially with 100% industrial
681 denatured alcohol (IDA), 90% IDA and 70% IDA and deionised water. Antigen retrieval was
682 performed in DAKO pH9 antigen retrieval solution using an EZ Retriever system (BioGenex)
683 at 98°C for 15 minutes. Samples were washed with deionised water and PBS. Endogenous
684 peroxidases were blocked by incubation with 10% hydrogen peroxide in PBS for 10 minutes.
685 Slides were incubated with Casein for 1 hour at 37°C. Anti-OMD primary antibody was added
686 at 1:50 for 1 hour at 37°C. Slides were washed three times with PBS. Envision anti-mouse
687 secondary fluorescent antibody was added to slides for 30 minutes at 37°C. Slides were
688 washed twice with PBS. DAB was added (1 drop DAB in 1ml diluent) to slides for 5 minutes
689 before washing with deionised water and staining for 10 seconds with Gills I haemotoxylin.
690 Slides were washed with water, 70% IDA, 90% IDA and 100% IDA. Slides were air-dried and
691 scanned as above. Analysis for our cohort of patient samples was performed by consultant
692 pathologist Nisha Ali who selected five fields of view per slide and assessed the cell types that
693 were positively stained within each field of view based on morphology. Haemotoxylin and
694 Eosin staining of breast cancer patient samples was performed by Cancer Research UK
695 Manchester Institute Histology facility and epithelial percentage in each section was calculated
696 by pathologist Nisha Ali who identified epithelial cells by morphology and estimate the area
697 covered by epithelial cells compared to the total size of tissue on the slide. Analysis of primary
698 tumours from patients recruited into the trial [29] were performed on TMAs constructed for the
699 purpose of this study. Identification of positively stained areas was conducted using QuPath
700 version 0.2.3 using the positive pixel count module.

701 **Quantitative RT-PCR**

702 RNA was isolated from cells at 70-90% confluency using a ReliaPrep™ RNA Cell Miniprep
703 system according to manufacturer's instructions. Isolated RNA was reverse transcribed using
704 a GoScript™ Reverse Transcription System according to manufacturer's instructions. Specific
705 genes within complementary DNA (cDNA) were amplified using gene-specific primers and a

706 2X SYBR Green mixture. The qPCR machines used were the Agilent Mx3000P and the Aria
707 Mx Real-time qPCR System. Relative expression was quantified using the Delta-Delta-CT
708 method with β-actin as a housekeeping gene.

709 **Cell Lysis and Immunoblotting**

710 Cell lines were lysed with SDS sample buffer supplemented with beta mercaptoethanol and
711 samples were heated at 95 degrees for 30 minutes. Patient samples were pelleted and lysed
712 at 4°C on a rotating wheel for 1 hr. Lysates were centrifuged at 12,000g to remove debris.
713 Supernatant was quantified using Pierce™ BCA Protein Assay (ThermoFisher) following the
714 manufacturers protocol. Lysates were normalised to the same concentration and boiled at
715 95°C for 5 minutes. All proteins were resolved by SDS-PAGE and transferred onto
716 nitrocellulose membranes. Specific antibodies were used to probe for proteins of interest and
717 peroxidase-labelled secondary antibodies recognised primary antibodies. An enhanced
718 chemiluminescence kit (Biorad) was used to assess expression and blots were visualised
719 using a Universal Hood II Gel Molecular Imaging System (Biorad).

720 Densitometric analysis was performed using ImageJ (version 1.52). Tiff images exported from
721 ImageLab (Biorad) were converted to 8bit images. The square selection tool was used to
722 highlight the first lane and pressing Ctrl+1 allows the dimensions of this box to be moved over
723 each lane so that the selection size was identical. Background was subtracted from the
724 generated base of the intensity curves using the line tool. The magic wand tool was used to
725 highlight the area underneath each peak providing a quantification of the area under the
726 intensity curve. Intensity values were divided by the loading control from the same lane to
727 normalise peak intensities.

728 **EdU Incorporation Assay**

729 Cells were incubated with 20μM 5-ethynyl-2'-deoxyuridine (EdU) for 4 hours at 37ºC. Cells
730 were fixed with 4% paraformaldehyde (PFA) in PBS and processed according to
731 manufacturer's instructions. After staining, cells were counterstained with 5ng/ml Hoechst

732 3342 for 30 minutes and counted using a Leica microscope system. Approximately 100
733 stained nuclei were counted before changing to a FITC filter and counting the number of cells
734 that also stained for Alexa488.

735 **Collagen Contractility Assay**

736 Flat-bottomed 96 well plates were coated with 100µl of sterile-filtered 3% bovine serum
737 albumin (BSA) in PBS for at least 1 hour at 37ºC before aspiration. 50,000 HFOB 1.19 cells
738 or 100,000 of MDA-MB-231, HMFU19 or 544R CAFs were resuspended in 10ul of their
739 respective medias. 7mg/ml Bovine type I collagen solution with 10% FCS at pH 7.7 was made.
740 90µl of the collagen mixture was mixed with 10µl cell suspension and added to a coated well
741 and allowed to set at 37ºC for 1 hour. 100µl of media was added. Any drugs or recombinant
742 protein used were added in this 100µl such as recombinant OMD on top of the collagen plug.
743 Samples were incubated at 37ºC for 72 hours before imaging using a GelCount image system.
744 Images were analysed using area measurements on ImageJ.

745 **Boyden Chamber Invasion Assay**

746 Matrigel (Corning) was diluted to 300µg/ml in PBS and 100µl was added to an 8µm pore 24
747 well Boyden chamber insert (Corning). Plates were incubated at 37ºC overnight to allow
748 Matrigel to set. 25,000 cells per well were added in 500µl starvation media to the top of the
749 chamber 750µl of complete media was added below the chamber. Cells were incubated for
750 24 hours at 37ºC. Matrigel was poured from the chamber. Cells were fixed with 400µl of 4%
751 PFA for 20 minutes, washed with PBS, permeabilised with 0.1% Triton x-100 in PBS for 15
752 minutes, washed with PBS and stained with 0.1% crystal violet (Sigma-Aldrich) in 4% PFA in
753 PBS. Wells were washed with PBS and water and air dried. Absorbance at 590nm was used
754 to assess crystal violet staining per well which shows the number of cells that migrated through
755 the Matrigel plug and the insert membrane.

756 **Scratch Wound Cell Migration Assay**

757 40,000 MDA-MB-231 cells and 70,000 MCF-7 cells per well were plated in a flat-bottomed 96
758 well plate (Corning) and incubated at 37°C overnight to reach 100% confluence. Cells were
759 treated for 2 hours at 37°C with 10µg/ml mitomycin (Fisher Scientific) to prevent cell
760 proliferation. An Essen bioscience woundmaker was used to create an even scratch in each
761 well. Wells were washed with PBS and starvation media was added to each well. Recombinant
762 OMD or CDK1 or CDK4,6 inhibitors were added to starvation media. Conditioned media was
763 added in place of starvation media for conditioned media experiments. Images of each well
764 were taken every hour using an Incucyte S3 system with 4x objective. Wound density at every
765 hour over 48 hours was measured using ImageJ. The final wound density at 48 hours post-
766 scratch was used as a measure of the degree of migration of cells.

767 **Mammosphere Assays**

768 Flat-bottomed 6 well plates were coated with polyHEMA for 48 hours at 40°C until dry.
769 Trypsinised cells were disaggregated to a single cell suspension by passing cells three times
770 through a 25-gauge needle. 3000 disaggregated cells per well were plated into 2ml
771 mammosphere media (DMEM/F12 with B27 supplement and 20ng/ml EGF (Sigma-Aldrich))
772 and cultured for 5 days in suspension before counting mammosphere greater than 50µm in
773 size (width and height). Mammosphere forming efficiency as counted by dividing the number
774 of mammosphere formed by the number of cells plated initially. Primary mammosphere were
775 trypsin-digested and needle disaggregated as above and were plated at a density of 3000
776 cells per well into new polyHEMA-coated plates in 2ml of mammosphere media and incubated
777 for 5 days in suspension. Mammosphere self-renewal percentage was calculated by dividing
778 the number of secondary mammosphere that formed over the number of primary
779 mammosphere and multiplying by 100.

780 **Alkaline Phosphatase Activity Assay**

781 A p-Nitrophenyl Phosphate, Disodium Salt (PnPP) standard curve of 33µM, 67µM, 100µM,
782 133µM and 167µM in assay buffer was produced as a substrate curve for alkaline

783 phosphatase modification. HFOB 1.19 cells were trypsinised, pelleted, resuspended in PBS
784 and 50,000 cells were pelleted and 50µl of assay buffer and 50µl of lysis buffer (20mM Tris-
785 HCl pH 8.0, 160mM NaCl, 1mM $CaCl_2$, 1% Triton-X-100) and pipetted up and down 20 times
786 to lyse cells. Samples were centrifuged at 18000xg for 15 minutes at 4°C to pellet insoluble
787 material. 20µl of each supernatant was added to 60µl of assay buffer and 50µl 5mM PnPP in
788 a 96 well plate. 10µl of alkaline phosphatase enzyme was added to each standard well and
789 mixed by pipetting up and down. Samples were incubated at room temperature in the dark for
790 1 hour. 20µl of stop solution was added to each sample and optical density at 405nm was
791 measured using a plate reader (Agilent/Biotek). Alkaline phosphatase activity was measured
792 by comparing OD at 405nm to the standard curve of known alkaline phosphatase activity. Data
793 were presented as µmol/min/ml of substrate modified by alkaline phosphatase per minute per
794 ml of reaction mixture.

795 **Alizarin Red Staining**

796 HFOB 1.19 cells were cultured at 34°C for undifferentiated cells or 39°C for differentiation.
797 Media was changed every 2 days, including treatments such as recombinant OMD.
798 Conditioned media was added 1:1 with HFOB 1.19 media. When cells reached 80% (for 34°C
799 condition) or after 7 days (for 39°C condition) they were fixed with ethanol, washed with PBS
800 and stained with 40mM Alizarin red pH 4.2 in water for 1 hour at room temperature on a rocker.
801 Plates were washed with 95% ethanol until all unbound stain was removed. Plates were
802 scanned on a GelCount plate imager (Oxford Optronix) and the percentage area stained with
803 calcium per well was calculated using ImageJ.

804 **Bone Resorption Assay**

805 Bovine cortical bone slices were UV-sterilised and added to a flat-bottomed 96 well plate.
806 50,000 RAW 264.7 cells (undifferentiated or RANKL-differentiated) were added to each well
807 in 100µl media (complete media or conditioned media) including any DMSO or recombinant
808 OMD treatment required. Cells were cultured for 7 days and media was changed every 48-72

809 hours. Bone discs were fixed in 4% PFA in PBS for 10 minutes at room temperature. Samples
810 were stained with 1% toluidine blue in water for 4 minutes. Samples were sonicated at 25%
811 amplitude (50-60Hz) for 30 minutes in deionised water to remove bound cells which may be
812 blocking pits from being stained. Samples were stained again with 1% toludine blue in water
813 for 4 minutes. Samples were washed with deionised water, air dried and imaged using a Leica
814 M205 Stereo Fluorescence System at 0.912X magnification. Resorption pits were quantified
815 and measured using ImageJ where pits of a minimum of 0.01mm in width and length were
816 counted.

817 **Alamar Blue Cell Viability Assay**

818 U-bottomed 96 well plates were coated with 100µl polyHEMA for 48 hours at 40ºC until dry.
819 10,000 cells were plated in DMEM (for MDA-MB-231 cells) with 10% FCS, 1% Pen-Strep,
820 1mM Sodium Pyruvate or Advanced DMEM/F12 with FCS, 1ug/ml hydrocortisone and
821 20ng/ml EGF (for cells from metastatic effusion samples). 10µl alamar blue reagent was added
822 to each well and incubated for 4 hours at 37ºC. Fluorescence at 590nm was measured using
823 a VarioSkan Lux with SkanIT 6.1 software. At least 3 biological replicates were performed for
824 each condition for MDA-MB-231 cells and 3 technical replicates were performed for effusion
825 samples from one effusion drain per patient.

826 **Quantification of OMD in conditioned medium and metastatic fluids**

827 Conditioned medium (CM) was derived using serum free medium. 231-OMD, HMFU19 and
828 544R were cultured at 37°C and 5% CO_2 for 72hrs. At 24-hour intervals, the medium was
829 collected, pooled, and replaced with fresh serum free medium. The CM was then centrifuged
830 at 500g for 20 minutes and then concentrated using Vivaspin Turbo 15 Centrifugal
831 Concentrator 10 kDa PES tubes. The resulting samples and the metastatic fluids derived from
832 ascitic drains and pleural effusions were then analysed using a Human
833 Osteoadherin/Osteomodulin ELISA Kit following manufacturer's instructions Briefly, 100 µL of
834 concentrated medium from each condition was added and incubated for 2.5hrs. Following

835 washing, 100 μL of biotinylated antibody was incubated for 1hr. The wells were washed again
836 and 100 μL of Streptavidin was added and incubated for 45mins. Following washing, 100 μL
837 of TMB One-Step Substrate Reagent was added and incubated in the dark for 30mins. Finally,
838 50 μL of stop solution was added and read at 450 nm.
839
840 **Statistics**

841 Experiments were performed in at least three independent biological triplicates. One-way
842 ANOVAs with Dunnett's multiple comparisons test were used to determine significance
843 between 3 or more experimental conditions. In experiments where the data was not normal,
844 Kruskal-Wallis with Dunn's multiple comparisons test was used to determine significance
845 between 3 or more experimental conditions. Student's t tests were used to determine
846 significance between two experimental conditions.

847
848
849
850
851
852
853
854
855
856
857
858
859
860
861
862

863 ## Figure Legends

864 **Figure 1.** Proteomics analysis identifies enrichment of OMD in samples from patients who
865 developed bone metastases **A,** Workflow of the proteomics and phosphoproteomics analysis
866 of patient-derived samples. The characteristics of samples and the numbers of proteins and
867 phosphorylated sites identified are indicated. Tissue and mouse images were downloaded
868 from SmartServier Medical Art. **B, C,** Volcano plots showing differentially expressed proteins
869 (B) or phosphorylated sites (C) based on Limma *p* value <0.05, Log2 Fold change >1.5
870 between metastatic and non-metastatic samples. Proteins or sites upregulated in patients who
871 developed metastases are in orange while proteins and sites downregulated in patients who
872 developed metastases are in blue. Proteins and phosphorylated sites previously associated
873 with breast cancer metastasis regulation are labelled (see Table S7). **D,** KEGG and GO terms
874 enrichment analysis of differentially regulated proteins and phosphorylated sites between
875 metastatic and non-metastatic samples from B and C. Adjusted *p* values are generated using
876 Fisher's exact test with Benjamini-Hochberg correction. **E**, Osteomodulin (OMD) log2
877 normalised protein intensity in non-metastatic patients, metastatic patients, patients who
878 developed bone metastases or patients who developed metastases at any other sites not
879 including bone. Data represent mean +/- SEM of 15 non-metastatic samples compared to 20
880 metastatic samples, and 12 bone-metastatic samples compared to 8 non-bone metastatic
881 samples (Limma *p* values ** <0.01, *** <0.001, **** <0.0001) and are visualised in the same
882 graph. **F,** OMD mRNA levels in bone metastasis and in metastases to other organs from the
883 GEO datasets (https://www.ncbi.nlm.nih.gov/pmc/articles/PMC6424882/). Data (37 bone
884 metastatic patient samples, 148 other metastatic site patient samples) are represented as
885 mean (Limma *p* values with Benjamini-Hochberg False Discovery Rate Correction <
886 0.0001****). See also Figures S1-2, Tables S1-7.

887 **Figure 2.** OMD regulates cell migration *in vitro* in both ER+ and ER- cell line models of breast
888 cancer. **A, B,** Immunoblotting analysis with the indicated antibodies of total lysates from MDA-
889 MB-231 cells stably transfected with mApple (231-mA) or an OMD-T2A-mApple construct

890 (231-OMD) and grown in complete or starved medium (A) and of conditioned medium from
891 the same cells (B) N=3 independent biological replicates. **C,** Cell migration of 231-mA (grey),
892 231-OMD (red), 231-mA treated with 10, 100 or 1000 ng/ml of rOMD assessed by wound
893 density (percentage of the wound filled with cells 48hrs post-scratch compared to time zero).
894 **D,** Representative images from C. Scale bar = 1mm. **E,** Cell migration of MCF-7 (orange)
895 treated with 10, 100 or 1000 ng/ml of rOMD assessed by wound density (percentage of the
896 wound filled with cells 48hrs post-scratch compared to time zero). **F,** Representative images
897 from E. Scale bar = 1mm. **C, E,** Data represents the mean +/- SEM of N = 3 independent
898 biological replicates, each including at least 3 technical triplicates. p =< 0.05*, < 0.01**, <
899 0.001***, < 0.0001**** (One Way ANOVA with Dunnett's Multiple Comparison Test, compared
900 to untreated control). **D, F,** The yellow lines indicate wound gap at 48h. See also Figures S3-
901 4.

902 **Figure 3.** OMD is expressed by cancer-associated fibroblasts in patient samples and
903 fibroblast-derived conditioned media drives cell migration. **A,** Single cell RNAseq UMAP
904 analysis of 26 primary breast cancer samples showcasing all the cell types[78]. **B,** UMAP
905 analysis of OMD RNA levels from the dataset in A. UMAP plot of OMD expression across all
906 cell types analysed using CELLxGENE[28]. Black circle highlights the fibroblast population as
907 containing cells expressing OMD. **C,** ELISA-based quantification of OMD secretion from
908 conditioned media (CM) collected from 231-OMD and 544R cells. Data represents the mean
909 +/- SEM of N = 3 independent biological replicates, each including 2 technical replicates. **D,**
910 Cell migration of 231-mA cells treated with 1000 ng/mL rOMD or with CM derived from 544R
911 (blue) assessed by wound density (percentage of the wound filled with cells 48hrs post-scratch
912 compared to time zero). **E,** Representative images from D. Scale bar = 1mm. **F,** Cell migration
913 of MCF-7 treated with 1000 ng/mL rOMD or with CM derived from 544R (blue) assessed by
914 wound density (percentage of the wound filled with cells 48hrs post-scratch compared to time
915 zero). **G,** Representative images from F. Scale bar = 1mm. **D, F,** Data represents the mean
916 +/- SEM of N = 3 independent biological replicates, each including at least 3 technical

917 triplicates (Mann-Whitney Test). **E, G,** The yellow lines indicate wound gap at 48hrs. See also
918 Figure S5.

919 **Figure 4.** Phosphoproteomics identifies the OMD-CDK1 axis in breast cancer and patient-
920 derived samples. **A,** Volcano plot showing differentially regulated phosphorylated sites in 231-
921 OMD cells compared to 231-mApple cells based on Limma *p* value <0.05, Log2 Fold Change
922 >1. Orange, upregulated in 231-OMD; blue, downregulated in 231-OMD; black text,
923 downregulated sites in 231-OMD compared to 231-mApple and in 231-Bo OMD compared to
924 231-Bo; red text, sites with metastasis-associated functions according to Phosphosite plus. **B,**
925 **C,** Immunoblotting analysis with indicated antibodies of 231-mApple, 231-OMD, 231-Bo and
926 231-Bo OMD cell lysates (B) followed by quantification via densitometry and normalisation to
927 vinculin (C). Data is presented as the ratio between the intensity of CDK1 phosphorylated on
928 Y15 and the intensity of the loading control. Values were calculated using ImageJ and are
929 presented relative to 231-mA band intensity. N = 3 independent biological replicates p =<
930 0.05*, < 0.01**, < 0.001***, < 0.0001**** (Student's t-test). **D, E,** Expression of OMD and of
931 phosphorylated CDK1 on Y15 from two independent proteomics and phosphoproteomics
932 datasets [11,33]. Data is presented as mean +/- SEM of Log2 iTRAQ ratios (N = 83) and Log TMT
933 ratios (N = 122), respectively, and compared to an internal standard. *p* =< 0.05*, < 0.01**, <
934 0.001***, < 0.0001**** (Student's *t*-test). **F, G,** Kaplan-Meyer analysis of distant metastasis
935 free survival with high and low expression of OMD and CDK1 in all breast cancer patients (F)
936 and those with the estrogen receptor positive (ER+) subtype (G) for 180 months. See also
937 Figures S6, Tables S6-12.

938 **Figure 5.** CDK1 regulates cell migration and viability downstream of OMD *in vitro*. **A,** Cell
939 migration of 231-mA and 231-OMD treated with either DMSO, 10 μM RO-3306 (CDK1i) or 10
940 μM Palbociclib (CDK4/6i) assessed by wound closure and measured by wound density. **B,**
941 **C,** Cell migration of 231-mA (B) and MCF-7 (C) cells treated with either DMSO or 1000 ng/mL
942 rOMD in the presence or absence of 10 μM RO-3306 assessed by wound closure over 48hrs
943 and measured by wound density. **D,** Cell migration of 231-mA and MCF-7 cells treated with

944 the 544R conditioned medium (CM) in the presence or absence of 10 μM RO-3306. **E, F,**
945 Relative viability of 231-mA (E) and MCF-7 (F) following treatment with 10 μM CDK1i. Data is
946 represented as mean +/- SEM of N >= 3 independent biological replicates. *p* =< 0.05*, < 0.01**,
947 < 0.001***, < 0.0001**** (Student's *t*-test). **G,** Table showing the 5 patients from which
948 metastatic effusions were collected along with their clinical characteristics and metastatic sites
949 at time of collection. BB7210 had two drains collected at different timepoints (T1, T3). ER –
950 Estrogen receptor, PR – Progesterone Receptor, HER2 – Human Epidermal Receptor 2. **H,**
951 ELISA-based quantification of OMD in the metastatic fluid of the patients described in G. Data
952 represents the mean +/- SEM of N = 1, each including two technical replicates. **I,**
953 Immunoblotting analysis with the indicated antibodies of total lysates from fresh frozen
954 samples derived from the patients illustrated in G, with the exception of BB3RC82. **J,** Relative
955 viability of 6 metastatic fluid samples following treatment with 10 μM CDK1i. Data is
956 represented as mean +/- SEM of N>= 1 independent biological replicates. *p* =< 0.05*, < 0.01**,
957 < 0.001***, < 0.0001**** (Student's *t*-test). **A, B, C,** Data represent the percentage of the
958 wound filled with cells 48 hours post-scratch. N = 3 biologically independent replicates. p =<
959 0.05*, < 0.01**, < 0.001***, < 0.0001**** (One Way ANOVA with Dunnett's Multiple
960 Comparison Test, compared to untreated control). See also Figures S7, Tables S13-14.

961 **Figure 6.** The OMD-CDK1 axis drives bone metastasis and bone colonization *in vivo*. **A,**
962 Diagram illustrating the set-up of the *in vivo* experiments in athymic nude mice following the
963 intracardiac injection of 100,000 231-mA, 231-OMD, or 231-Bo cells (i) and of 100,000 231-
964 OMD cells followed by treatment with 4 mg/mL CDK1i (ii). Figure designed using
965 Biorender.com. **B,** Number of metastatic lung lesions of over 100 μm in diameter (in at least 1
966 dimension) following intracardiac injection in N = 4 mice per cell line. **C,** Number of cytokeratin
967 19 (CK19)-positive human cells identified in cytospun bone flushes from the same mice. *p* =<
968 0.05*, < 0.01**, < 0.001***, < 0.0001**** (Mean +/- SEM, Student's *t*-test, each compared to
969 231-mA). **D,** Representative images from C where red arrows indicated CK19-positive cells.
970 **E,** Number of CK19-positive human cells identified in cytospun bone flushes following

971 intracardiac injection and treatment with CDK1 inhibitor 4 mg/kg RO-3306 or vehicle control 3
972 times per week for 25 days in N = 4 mice per condition. p =< 0.05*, < 0.01**, < 0.001***, <
973 0.0001**** (Mean +/- SEM, Student's *t*-test, each compared to 231-mA). **F,** Representative
974 images from E where red arrows indicate CK19-positive cells.

975

976 **References**

977 1. Nolan, E., Lindeman, G.J., and Visvader, J.E. (2023). Deciphering breast cancer: from
978 biology to the clinic. Cell *186*, 1708-1728. 10.1016/j.cell.2023.01.040.
979 2. Riggio, A.I., Varley, K.E., and Welm, A.L. (2021). The lingering mysteries of metastatic
980 recurrence in breast cancer. British Journal of Cancer *124*, 13-26. 10.1038/s41416-
981 020-01161-4.
982 3. Fornetti, J., Welm, A.L., and Stewart, S.A. (2018). Understanding the Bone in Cancer
983 Metastasis. J Bone Miner Res *33*, 2099-2113. 10.1002/jbmr.3618.
984 4. Mundy, G.R. (2002). Metastasis to bone: causes, consequences and therapeutic
985 opportunities. Nat Rev Cancer *2*, 584-593. 10.1038/nrc867.
986 5. Satcher, R.L., and Zhang, X.H. (2022). Evolving cancer-niche interactions and
987 therapeutic targets during bone metastasis. Nat Rev Cancer *22*, 85-101.
988 10.1038/s41568-021-00406-5.
989 6. Zhang, W., Bado, I.L., Hu, J., Wan, Y.W., Wu, L., Wang, H., Gao, Y., Jeong, H.H., Xu,
990 Z., Hao, X., et al. (2021). The bone microenvironment invigorates metastatic seeds for
991 further dissemination. Cell *184*, 2471-2486 e2420. 10.1016/j.cell.2021.03.011.
992 7. Coleman, R.E., and Rubens, R.D. (1987). The clinical course of bone metastases from
993 breast cancer. Br J Cancer *55*, 61-66. 10.1038/bjc.1987.13.
994 8. Parsons, J., and Francavilla, C. (2019). 'Omics Approaches to Explore the Breast
995 Cancer Landscape. Front Cell Dev Biol *7*, 395. 10.3389/fcell.2019.00395.
996 9. Paul, M.R., Pan, T.C., Pant, D.K., Shih, N.N., Chen, Y., Harvey, K.L., Solomon, A.,
997 Lieberman, D., Morrissette, J.J., Soucier-Ernst, D., et al. (2020). Genomic landscape
998 of metastatic breast cancer identifies preferentially dysregulated pathways and targets.
999 J Clin Invest *130*, 4252-4265. 10.1172/jci129941.
1000 10. Zhang, Y., He, W., and Zhang, S. (2019). Seeking for Correlative Genes and Signaling
1001 Pathways With Bone Metastasis From Breast Cancer by Integrated Analysis. Front
1002 Oncol *9*, 138. 10.3389/fonc.2019.00138.

1003 11. Krug, K., Jaehnig, E.J., Satpathy, S., Blumenberg, L., Karpova, A., Anurag, M., Miles,
1004 G., Mertins, P., Geffen, Y., Tang, L.C., et al. (2020). Proteogenomic Landscape of
1005 Breast Cancer Tumorigenesis and Targeted Therapy. Cell *183*, 1436-1456.e1431.
1006 10.1016/j.cell.2020.10.036.
1007 12. Anurag, M., Jaehnig, E.J., Krug, K., Lei, J.T., Bergstrom, E.J., Kim, B.-J., Vashist, T.D.,
1008 Tran Huynh, A.M., Dou, Y., Gou, X., et al. (2022). Proteogenomic markers of
1009 chemotherapy resistance and response in triple negative breast cancer. Cancer
1010 Discovery, CD-22-0200. 10.1158/2159-8290.CD-22-0200.
1011 13. Zagorac, I., Fernandez-Gaitero, S., Penning, R., Post, H., Bueno, M.J., Mouron, S.,
1012 Manso, L., Morente, M.M., Alonso, S., Serra, V., et al. (2018). In vivo
1013 phosphoproteomics reveals kinase activity profiles that predict treatment outcome in
1014 triple-negative breast cancer. Nature Communications *9*, 3501. 10.1038/s41467-018-
1015 05742-z.
1016 14. Satpathy, S., Jaehnig, E.J., Krug, K., Kim, B.-J., Saltzman, A.B., Chan, D.W.,
1017 Holloway, K.R., Anurag, M., Huang, C., Singh, P., et al. (2020). Microscaled
1018 proteogenomic methods for precision oncology. Nature Communications *11*, 532.
1019 10.1038/s41467-020-14381-2.
1020 15. Ramstad, V.E., Franzen, A., Heinegard, D., Wendel, M., and Reinholt, F.P. (2003).
1021 Ultrastructural distribution of osteoadherin in rat bone shows a pattern similar to that
1022 of bone sialoprotein. Calcif Tissue Int *72*, 57-64. 10.1007/s00223-002-2047-9.
1023 16. Sommarin, Y., Wendel, M., Shen, Z., Hellman, U., and Heinegard, D. (1998).
1024 Osteoadherin, a cell-binding keratan sulfate proteoglycan in bone, belongs to the
1025 family of leucine-rich repeat proteins of the extracellular matrix. J Biol Chem *273*,
1026 16723-16729. 10.1074/jbc.273.27.16723.
1027 17. Watson, J., Ferguson, H.R., Brady, R.M., Ferguson, J., Fullwood, P., Mo, H., Bexley,
1028 K.H., Knight, D., Howell, G., Schwartz, J.M., et al. (2022). Spatially resolved
1029 phosphoproteomics reveals fibroblast growth factor receptor recycling-driven

1030 regulation of autophagy and survival. Nat Commun *13*, 6589. 10.1038/s41467-022-
1031 34298-2.
1032 18. Song, K., Yu, Z., Zu, X., Li, G., Hu, Z., and Xue, Y. (2022). Collagen Remodeling along
1033 Cancer Progression Providing a Novel Opportunity for Cancer Diagnosis and
1034 Treatment. Int J Mol Sci *23*. 10.3390/ijms231810509.
1035 19. Roudier, M.P., Winters, B.R., Coleman, I., Lam, H.M., Zhang, X., Coleman, R., Chéry,
1036 L., True, L.D., Higano, C.S., Montgomery, B., et al. (2016). Characterizing the
1037 molecular features of ERG-positive tumors in primary and castration resistant prostate
1038 cancer. Prostate *76*, 810-822. 10.1002/pros.23171.
1039 20. Kojima, K., Shimanuki, M., Shikami, M., Andreeff, M., and Nakakuma, H. (2009).
1040 Cyclin-dependent kinase 1 inhibitor RO-3306 enhances p53-mediated Bax activation
1041 and mitochondrial apoptosis in AML. Cancer Sci *100*, 1128-1136. 10.1111/j.1349-
1042 7006.2009.01150.x.
1043 21. O'Hare, M.J., Bond, J., Clarke, C., Takeuchi, Y., Atherton, A.J., Berry, C., Moody, J.,
1044 Silver, A.R., Davies, D.C., Alsop, A.E., et al. (2001). Conditional immortalization of
1045 freshly isolated human mammary fibroblasts and endothelial cells. Proc Natl Acad Sci
1046 U S A *98*, 646-651. 10.1073/pnas.98.2.646.
1047 22. Harris, S.A., Enger, R.J., Riggs, L.B., and Spelsberg, T.C. (1995). Development and
1048 characterization of a conditionally immortalized human fetal osteoblastic cell line.
1049 Journal of Bone and Mineral Research *10*, 178-186.
1050 https://doi.org/10.1002/jbmr.5650100203.
1051 23. Lampiasi, N., Russo, R., Kireev, I., Strelkova, O., Zhironkina, O., and Zito, F. (2021).
1052 Osteoclasts Differentiation from Murine RAW 264.7 Cells Stimulated by RANKL:
1053 Timing and Behavior. Biology (Basel) *10*. 10.3390/biology10020117.
1054 24. Papadaki, V., Asada, K., Watson, J.K., Tamura, T., Leung, A., Hopkins, J., Dellett, M.,
1055 Sasai, N., Davaapil, H., Nik-Zainal, S., et al. (2020). Two Secreted Proteoglycans,
1056 Activators of Urothelial Cell-Cell Adhesion, Negatively Contribute to Bladder Cancer
1057 Initiation and Progression. Cancers (Basel) *12*. 10.3390/cancers12113362.

1058 25. Macedo, F., Ladeira, K., Pinho, F., Saraiva, N., Bonito, N., Pinto, L., and Goncalves,
1059 F. (2017). Bone Metastases: An Overview. Oncol Rev *11*, 321.
1060 10.4081/oncol.2017.321.
1061 26. Tashima, T., Nagatoishi, S., Sagara, H., Ohnuma, S., and Tsumoto, K. (2015).
1062 Osteomodulin regulates diameter and alters shape of collagen fibrils. Biochem Biophys
1063 Res Commun *463*, 292-296. 10.1016/j.bbrc.2015.05.053.
1064 27. Bos, P.D., Zhang, X.H., Nadal, C., Shu, W., Gomis, R.R., Nguyen, D.X., Minn, A.J.,
1065 van de Vijver, M.J., Gerald, W.L., Foekens, J.A., and Massagué, J. (2009). Genes that
1066 mediate breast cancer metastasis to the brain. Nature *459*, 1005-1009.
1067 10.1038/nature08021.
1068 28. Program, C.Z.I.C.S., Abdulla, S., Aevermann, B., Assis, P., Badajoz, S., Bell, S.M.,
1069 Bezzi, E., Cakir, B., Chaffer, J., Chambers, S., et al. (2025). CZ CELLxGENE Discover:
1070 a single-cell data platform for scalable exploration, analysis and modeling of
1071 aggregated data. Nucleic Acids Res *53*, D886-D900. 10.1093/nar/gkae1142.
1072 29. Coleman, R., Cameron, D., Dodwell, D., Bell, R., Wilson, C., Rathbone, E., Keane, M.,
1073 Gil, M., Burkinshaw, R., Grieve, R., et al. (2014). Adjuvant zoledronic acid in patients
1074 with early breast cancer: final efficacy analysis of the AZURE (BIG 01/04) randomised
1075 open-label phase 3 trial. Lancet Oncol *15*, 997-1006. 10.1016/S1470-2045(14)70302-
1076 X.
1077 30. Hornbeck, P.V., Kornhauser, J.M., Tkachev, S., Zhang, B., Skrzypek, E., Murray, B.,
1078 Latham, V., and Sullivan, M. (2012). PhosphoSitePlus: a comprehensive resource for
1079 investigating the structure and function of experimentally determined post-translational
1080 modifications in man and mouse. Nucleic Acids Res *40*, D261-270.
1081 10.1093/nar/gkr1122.
1082 31. Belguise, K., Milord, S., Galtier, F., Moquet-Torcy, G., Piechaczyk, M., and Chalbos,
1083 D. (2012). The PKCθ pathway participates in the aberrant accumulation of Fra-1
1084 protein in invasive ER-negative breast cancer cells. Oncogene *31*, 4889-4897.
1085 10.1038/onc.2011.659.

1086 32. Potapova, T.A., Daum, J.R., Byrd, K.S., and Gorbsky, G.J. (2009). Fine tuning the cell
1087 cycle: activation of the Cdk1 inhibitory phosphorylation pathway during mitotic exit. Mol
1088 Biol Cell *20*, 1737-1748. 10.1091/mbc.e08-07-0771.
1089 33. Mertins, P., Mani, D.R., Ruggles, K.V., Gillette, M.A., Clauser, K.R., Wang, P., Wang,
1090 X., Qiao, J.W., Cao, S., Petralia, F., et al. (2016). Proteogenomics connects somatic
1091 mutations to signalling in breast cancer. Nature *534*, 55-62. 10.1038/nature18003.
1092 34. Gyorffy, B. (2021). Survival analysis across the entire transcriptome identifies
1093 biomarkers with the highest prognostic power in breast cancer. Comput Struct
1094 Biotechnol J *19*, 4101-4109. 10.1016/j.csbj.2021.07.014.
1095 35. Vassilev, L.T., Tovar, C., Chen, S., Knezevic, D., Zhao, X., Sun, H., Heimbrook, D.C.,
1096 and Chen, L. (2006). Selective small-molecule inhibitor reveals critical mitotic functions
1097 of human CDK1. Proc Natl Acad Sci U S A *103*, 10660-10665.
1098 10.1073/pnas.0600447103.
1099 36. Rampersad, S.N. (2012). Multiple applications of Alamar Blue as an indicator of
1100 metabolic function and cellular health in cell viability bioassays. Sensors (Basel) *12*,
1101 12347-12360. 10.3390/s120912347.
1102 37. Krek, W., and Nigg, E.A. (1991). Differential phosphorylation of vertebrate p34cdc2
1103 kinase at the G1/S and G2/M transitions of the cell cycle: identification of major
1104 phosphorylation sites. EMBO J *10*, 305-316. 10.1002/j.1460-2075.1991.tb07951.x.
1105 38. Watase, C., Shiino, S., Shimoi, T., Noguchi, E., Kaneda, T., Yamamoto, Y., Yonemori,
1106 K., Takayama, S., and Suto, A. (2021). Breast Cancer Brain Metastasis-Overview of
1107 Disease State, Treatment Options and Future Perspectives. Cancers (Basel) *13*.
1108 10.3390/cancers13051078.
1109 39. Kycler, W.L., P. (2011). Surgical approach to pulmonary metastases from breast
1110 cancer. The Breast Journal *18*, 52-57.
1111 40. Makhmut, A., Qin, D., Hartlmayr, D., Seth, A., and Coscia, F. (2024). An Automated
1112 and Fast Sample Preparation Workflow for Laser Microdissection Guided

1113 Ultrasensitive Proteomics. Mol Cell Proteomics *23*, 100750.
1114 10.1016/j.mcpro.2024.100750.
1115 41. Petrosius, V., Aragon-Fernandez, P., Arrey, T.N., Woessman, J., Uresin, N., de Boer,
1116 B., Su, J., Furtwangler, B., Stewart, H., Denisov, E., et al. (2025). Quantitative Label-
1117 Free Single-Cell Proteomics on the Orbitrap Astral MS. Mol Cell Proteomics, 100982.
1118 10.1016/j.mcpro.2025.100982.
1119 42. Tashima, T., Nagatoishi, S., Caaveiro, J.M.M., Nakakido, M., Sagara, H., Kusano-Arai,
1120 O., Iwanari, H., Mimuro, H., Hamakubo, T., Ohnuma, S.I., and Tsumoto, K. (2018).
1121 Molecular basis for governing the morphology of type-I collagen fibrils by
1122 Osteomodulin. Commun Biol *1*, 33. 10.1038/s42003-018-0038-2.
1123 43. Hamaya, E., Fujisawa, T., and Tamura, M. (2019). Osteoadherin serves roles in the
1124 regulation of apoptosis and growth in MC3T3-E1 osteoblast cells. Int J Mol Med *44*,
1125 2336-2344. 10.3892/ijmm.2019.4376.
1126 44. Tan, Y., Demeter, M.R., Ruan, H., and Comb, M.J. (2000). BAD Ser-155
1127 Phosphorylation Regulates BAD/Bcl-XL Interaction and Cell Survival *. Journal of
1128 Biological Chemistry *275*, 25865-25869. 10.1074/jbc.M004199200.
1129 45. Lin, W., Zhu, X., Gao, L., Mao, M., Gao, D., and Huang, Z. (2021). Osteomodulin
1130 positively regulates osteogenesis through interaction with BMP2. Cell Death Dis *12*,
1131 147. 10.1038/s41419-021-03404-5.
1132 46. Giorello, M.B., Martinez, L.M., Borzone, F.R., Padin, M.D.R., Mora, M.F., Sevic, I.,
1133 Alaniz, L., Calcagno, M.L., Garcia-Rivello, H., Wernicke, A., et al. (2023). CD105
1134 expression in cancer-associated fibroblasts: a biomarker for bone metastasis in early
1135 invasive ductal breast cancer patients. Front Cell Dev Biol *11*, 1250869.
1136 10.3389/fcell.2023.1250869.
1137 47. Katsuno, Y., Hanyu, A., Kanda, H., Ishikawa, Y., Akiyama, F., Iwase, T., Ogata, E.,
1138 Ehata, S., Miyazono, K., and Imamura, T. (2008). Bone morphogenetic protein
1139 signaling enhances invasion and bone metastasis of breast cancer cells through Smad
1140 pathway. Oncogene *27*, 6322-6333. 10.1038/onc.2008.232.

1141 48. Sloan, E.K., Pouliot, N., Stanley, K.L., Chia, J., Moseley, J.M., Hards, D.K., and
1142 Anderson, R.L. (2006). Tumor-specific expression of alphavbeta3 integrin promotes
1143 spontaneous metastasis of breast cancer to bone. Breast Cancer Res *8*, R20.
1144 10.1186/bcr1398.
1145 49. Mirzakhanyan, Y., Jankevics, A., Scheltema, R.A., and Gershon, P.D. (2023).
1146 Combination of deep XLMS with deep learning reveals an ordered rearrangement and
1147 assembly of a major protein component of the vaccinia virion. mBio *14*, e0113523.
1148 10.1128/mbio.01135-23.
1149 50. Muller, M., Grabnitz, F., Barandun, N., Shen, Y., Wendt, F., Steiner, S.N., Severin, Y.,
1150 Vetterli, S.U., Mondal, M., Prudent, J.R., et al. (2021). Light-mediated discovery of
1151 surfaceome nanoscale organization and intercellular receptor interaction networks.
1152 Nat Commun *12*, 7036. 10.1038/s41467-021-27280-x.
1153 51. Ninomiya, K., Miyamoto, T., Imai, J., Fujita, N., Suzuki, T., Iwasaki, R., Yagi, M.,
1154 Watanabe, S., Toyama, Y., and Suda, T. (2007). Osteoclastic activity induces
1155 osteomodulin expression in osteoblasts. Biochem Biophys Res Commun *362*, 460-
1156 466. 10.1016/j.bbrc.2007.07.193.
1157 52. Rehn, A.P., Cerny, R., Sugars, R.V., Kaukua, N., and Wendel, M. (2008).
1158 Osteoadherin is upregulated by mature osteoblasts and enhances their in vitro
1159 differentiation and mineralization. Calcif Tissue Int *82*, 454-464. 10.1007/s00223-008-
1160 9138-1.
1161 53. Qiao, M., Shapiro, P., Fosbrink, M., Rus, H., Kumar, R., and Passaniti, A. (2006). Cell
1162 cycle-dependent phosphorylation of the RUNX2 transcription factor by cdc2 regulates
1163 endothelial cell proliferation. J Biol Chem *281*, 7118-7128. 10.1074/jbc.M508162200.
1164 54. Rajgopal, A., Young, D.W., Mujeeb, K.A., Stein, J.L., Lian, J.B., van Wijnen, A.J., and
1165 Stein, G.S. (2007). Mitotic control of RUNX2 phosphorylation by both CDK1/cyclin B
1166 kinase and PP1/PP2A phosphatase in osteoblastic cells. J Cell Biochem *100*, 1509-
1167 1517. 10.1002/jcb.21137.

1168 55. Li, X.Q., Lu, J.T., Tan, C.C., Wang, Q.S., and Feng, Y.M. (2016). RUNX2 promotes
1169 breast cancer bone metastasis by increasing integrin alpha5-mediated colonization.
1170 Cancer Lett *380*, 78-86. 10.1016/j.canlet.2016.06.007.
1171 56. Ran, R., Harrison, H., Syamimi Ariffin, N., Ayub, R., Pegg, H.J., Deng, W., Mastro, A.,
1172 Ottewell, P.D., Mason, S.M., Blyth, K., et al. (2020). A role for CBFbeta in maintaining
1173 the metastatic phenotype of breast cancer cells. Oncogene *39*, 2624-2637.
1174 10.1038/s41388-020-1170-2.
1175 57. Jones, M.C., Askari, J.A., Humphries, J.D., and Humphries, M.J. (2018). Cell adhesion
1176 is regulated by CDK1 during the cell cycle. Journal of Cell Biology *217*, 3203-3218.
1177 10.1083/jcb.201802088.
1178 58. Ratnayake, W.S., Apostolatos, C.A., Breedy, S., Dennison, C.L., Hill, R., and Acevedo-
1179 Duncan, M. (2021). Atypical PKCs activate Vimentin to facilitate prostate cancer cell
1180 motility and invasion. Cell Adh Migr *15*, 37-57. 10.1080/19336918.2021.1882782.
1181 59. Li, M., He, F., Zhang, Z., Xiang, Z., and Hu, D. (2020). CDK1 serves as a potential
1182 prognostic biomarker and target for lung cancer. J Int Med Res *48*, 300060519897508.
1183 10.1177/0300060519897508.
1184 60. Ravindran Menon, D., Luo, Y., Arcaroli, J.J., Liu, S., KrishnanKutty, L.N., Osborne,
1185 D.G., Li, Y., Samson, J.M., Bagby, S., Tan, A.C., et al. (2018). CDK1 Interacts with
1186 Sox2 and Promotes Tumor Initiation in Human Melanoma. Cancer Res *78*, 6561-6574.
1187 10.1158/0008-5472.Can-18-0330.
1188 61. Zheng, H.P., Huang, Z.G., He, R.Q., Lu, H.P., Dang, Y.W., Lin, P., Wen, D.Y., Qin,
1189 Y.Y., Luo, B., Li, X.J., et al. (2019). Integrated assessment of CDK1 upregulation in
1190 thyroid cancer. Am J Transl Res *11*, 7233-7254.
1191 62. Wu, C.X., Wang, X.Q., Chok, S.H., Man, K., Tsang, S.H.Y., Chan, A.C.Y., Ma, K.W.,
1192 Xia, W., and Cheung, T.T. (2018). Blocking CDK1/PDK1/β-Catenin signaling by CDK1
1193 inhibitor RO3306 increased the efficacy of sorafenib treatment by targeting cancer
1194 stem cells in a preclinical model of hepatocellular carcinoma. Theranostics *8*, 3737-
1195 3750. 10.7150/thno.25487.

1196 63. Paraghamian, S.E., Huang, Y., Hawkins, G.M., Fan, Y., Yin, Y., Zhang, X., Suo, H.,
1197 Zhou, C., and Bae-Jump, V.L. (2020). The Cdk1 inhibitor RO3306 has anti-tumorigenic
1198 effects in high-grade serous ovarian cancer. Gynecologic Oncology *159*, 88-89.
1199 10.1016/j.ygyno.2020.05.068.
1200 64. Wang, Q., Bode, A.M., and Zhang, T. (2023). Targeting CDK1 in cancer: mechanisms
1201 and implications. NPJ Precis Oncol *7*, 58. 10.1038/s41698-023-00407-7.
1202 65. Ji, H., Wang, J., Nika, H., Hawke, D., Keezer, S., Ge, Q., Fang, B., Fang, X., Fang, D.,
1203 Litchfield, D.W., et al. (2009). EGF-induced ERK activation promotes CK2-mediated
1204 disassociation of alpha-Catenin from beta-Catenin and transactivation of beta-Catenin.
1205 Mol Cell *36*, 547-559. 10.1016/j.molcel.2009.09.034.
1206 66. Kang, Y., Siegel, P.M., Shu, W., Drobnjak, M., Kakonen, S.M., Cordón-Cardo, C.,
1207 Guise, T.A., and Massagué, J. (2003). A multigenic program mediating breast cancer
1208 metastasis to bone. Cancer Cell *3*, 537-549. https://doi.org/10.1016/S1535-
1209 6108(03)00132-6.
1210 67. Holliday, D.L., Brouilette, K.T., Markert, A., Gordon, L.A., and Jones, J.L. (2009). Novel
1211 multicellular organotypic models of normal and malignant breast: tools for dissecting
1212 the role of the microenvironment in breast cancer progression. Breast Cancer Res *11*,
1213 R3. 10.1186/bcr2218.
1214 68. Kojima, Y., Acar, A., Eaton, E.N., Mellody, K.T., Scheel, C., Ben-Porath, I., Onder, T.T.,
1215 Wang, Z.C., Richardson, A.L., Weinberg, R.A., and Orimo, A. (2010). Autocrine TGF-
1216 beta and stromal cell-derived factor-1 (SDF-1) signaling drives the evolution of tumor-
1217 promoting mammary stromal myofibroblasts. Proc Natl Acad Sci U S A *107*, 20009-
1218 20014. 10.1073/pnas.1013805107.
1219 69. Collin-Osdoby, P., and Osdoby, P. (2012). RANKL-Mediated Osteoclast Formation
1220 from Murine RAW 264.7 cells. In Bone Research Protocols, M.H. Helfrich, and S.H.
1221 Ralston, eds. (Humana Press), pp. 187-202. 10.1007/978-1-61779-415-5_13.
1222 70. Wilcock, D.J., Badrock, A.P., Wong, C.W., Owen, R., Guerin, M., Southam, A.D.,
1223 Johnston, H., Telfer, B.A., Fullwood, P., Watson, J., et al. (2022). Oxidative stress from

1224 DGAT1 oncoprotein inhibition in melanoma suppresses tumor growth when ROS
1225 defenses are also breached. Cell Rep *39*, 110995. 10.1016/j.celrep.2022.110995.
1226 71. Cox, J., and Mann, M. (2008). MaxQuant enables high peptide identification rates,
1227 individualized p.p.b.-range mass accuracies and proteome-wide protein quantification.
1228 Nat Biotechnol *26*, 1367-1372. 10.1038/nbt.1511.
1229 72. Tyanova, S., Temu, T., Sinitcyn, P., Carlson, A., Hein, M.Y., Geiger, T., Mann, M., and
1230 Cox, J. (2016). The Perseus computational platform for comprehensive analysis of
1231 (prote)omics data. Nat Methods *13*, 731-740. 10.1038/nmeth.3901.
1232 73. Szklarczyk, D., Gable, A.L., Lyon, D., Junge, A., Wyder, S., Huerta-Cepas, J.,
1233 Simonovic, M., Doncheva, N.T., Morris, J.H., Bork, P., et al. (2019). STRING v11:
1234 protein-protein association networks with increased coverage, supporting functional
1235 discovery in genome-wide experimental datasets. Nucleic Acids Res *47*, D607-D613.
1236 10.1093/nar/gky1131.
1237 74. Kohl, M., Wiese, S., and Warscheid, B. (2011). Cytoscape: software for visualization
1238 and analysis of biological networks. Methods Mol Biol *696*, 291-303. 10.1007/978-1-
1239 60761-987-1_18.
1240 75. Schneider, C.A., Rasband, W.S., and Eliceiri, K.W. (2012). NIH Image to ImageJ: 25
1241 years of image analysis. Nat Methods *9*, 671-675. 10.1038/nmeth.2089.
1242 76. Bankhead, P., Loughrey, M.B., Fernandez, J.A., Dombrowski, Y., McArt, D.G., Dunne,
1243 P.D., McQuaid, S., Gray, R.T., Murray, L.J., Coleman, H.G., et al. (2017). QuPath:
1244 Open source software for digital pathology image analysis. Sci Rep *7*, 16878.
1245 10.1038/s41598-017-17204-5.
1246 77. Ritchie, M.E., Phipson, B., Wu, D., Hu, Y., Law, C.W., Shi, W., and Smyth, G.K. (2015).
1247 limma powers differential expression analyses for RNA-sequencing and microarray
1248 studies. Nucleic Acids Res *43*, e47. 10.1093/nar/gkv007.
1249 78. Wu, S.Z., Al-Eryani, G., Roden, D.L., Junankar, S., Harvey, K., Andersson, A.,
1250 Thennavan, A., Wang, C., Torpy, J.R., Bartonicek, N., et al. (2021). A single-cell and

1251 spatially resolved atlas of human breast cancers. Nat Genet *53*, 1334-1347.
1252 10.1038/s41588-021-00911-1.

1253

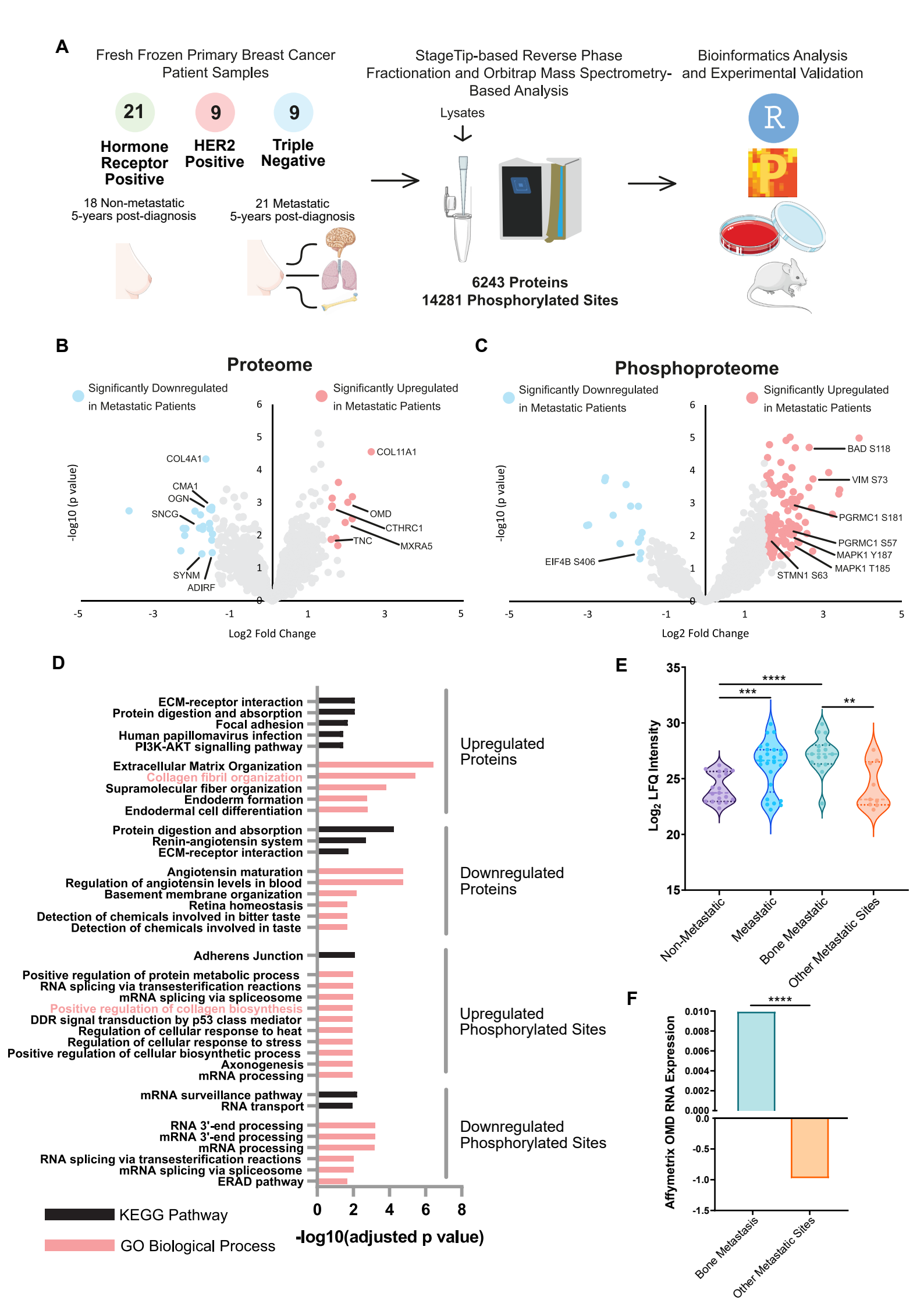
A
Fresh Frozen Primary Breast Cancer Patient Samples
21
Hormone Receptor Positive
9
HER2 Positive
9
Triple Negative
18 Non-metastatic 5-years post-diagnosis
21 Metastatic 5-years post-diagnosis
StageTip-based Reverse Phase Fractionation and Orbitrap Mass Spectrometry-Based Analysis
Lysates
6243 Proteins
14281 Phosphorylated Sites
Bioinformatics Analysis and Experimental Validation
B
Proteome
Significantly Downregulated in Metastatic Patients
Significantly Upregulated in Metastatic Patients
COL4A1
CMA1
OGN
SNCG
SYNM
ADIRF
COL11A1
OMD
CTHRC1
TNC
MXRA5
-log10 (p value)
Log2 Fold Change
C
Phosphoproteome
Significantly Downregulated in Metastatic Patients
Significantly Upregulated in Metastatic Patients
BAD S118
VIM S73
PGRMC1 S181
PGRMC1 S57
MAPK1 Y187
MAPK1 T185
STMN1 S63
EIF4B S406
-log10 (p value)
Log2 Fold Change
D
ECM-receptor interaction
Protein digestion and absorption
Focal adhesion
Human papillomavirus infection
PI3K-AKT signalling pathway
Extracellular Matrix Organization
Collagen fibril organization
Supramolecular fiber organization
Endoderm formation
Endodermal cell differentiation
Protein digestion and absorption
Renin-angiotensin system
ECM-receptor interaction
Angiotensin maturation
Regulation of angiotensin levels in blood
Basement membrane organization
Retina homeostasis
Detection of chemicals involved in bitter taste
Detection of chemicals involved in taste
Adherens Junction
Positive regulation of protein metabolic process
RNA splicing via transesterification reactions
mRNA splicing via spliceosome
Positive regulation of collagen biosynthesis
DDR signal transduction by p53 class mediator
Regulation of cellular response to heat
Regulation of cellular response to stress
Positive regulation of cellular biosynthetic process
Axonogenesis
mRNA processing
mRNA surveillance pathway
RNA transport
RNA 3'-end processing
mRNA 3'-end processing
mRNA processing
RNA splicing via transesterification reactions
mRNA splicing via spliceosome
ERAD pathway
Upregulated Proteins
Downregulated Proteins
Upregulated Phosphorylated Sites
Downregulated Phosphorylated Sites
KEGG Pathway
GO Biological Process
-log10(adjusted p value)
E
Log2 LFQ Intensity
Non-Metastatic
Metastatic
Bone Metastatic
Other Metastatic Sites
F
Affymetrix OMD RNA Expression
Bone Metastasis
Other Metastatic Sites

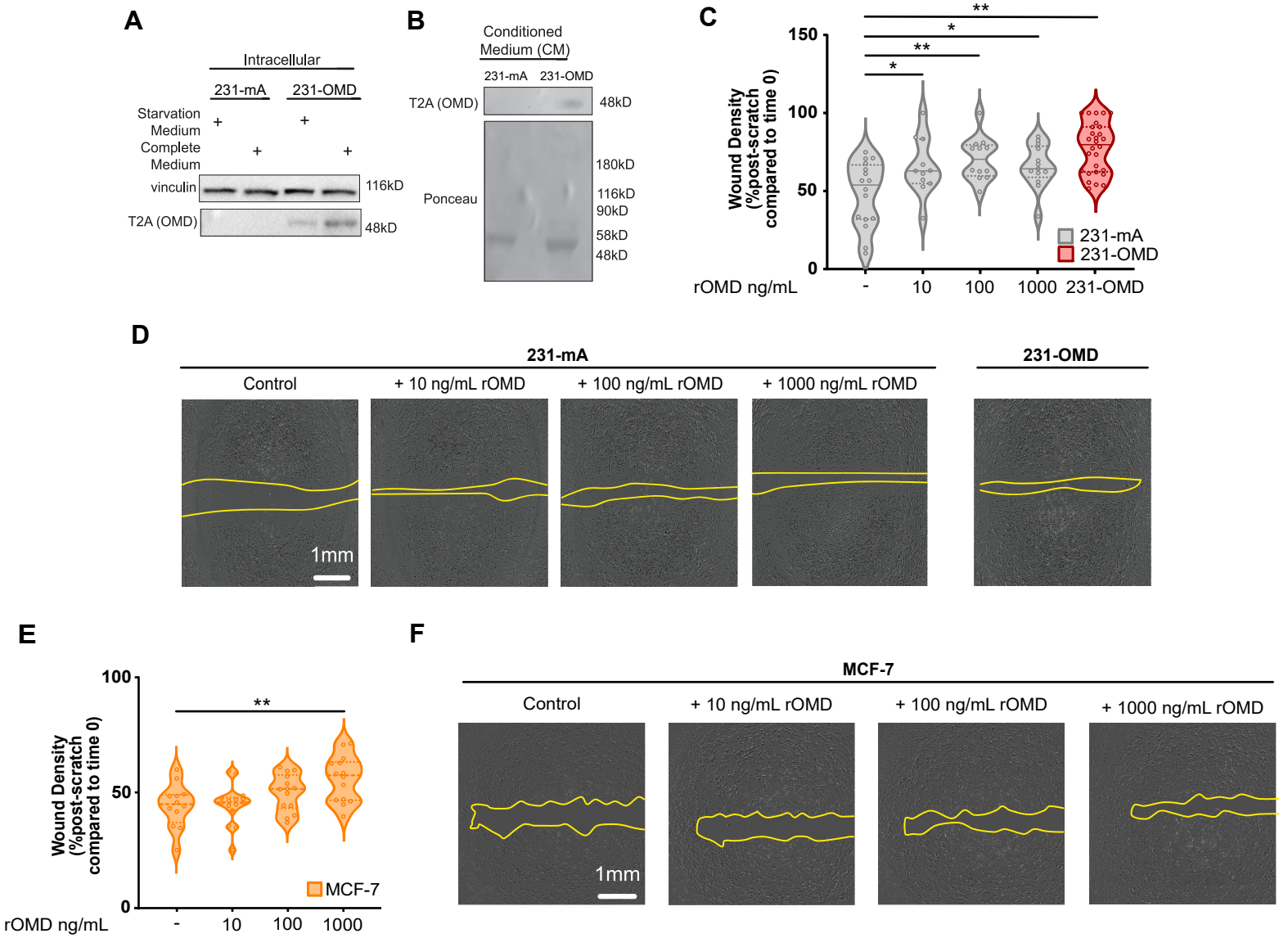
A
Intracellular
231-mA
231-OMD
Starvation Medium
Complete Medium
vinculin
116kD
T2A (OMD)
48kD
B
Conditioned Medium (CM)
231-mA
231-OMD
T2A (OMD)
48kD
Ponceau
180kD
116kD
90kD
58kD
48kD
C
Wound Density (%post-scratch compared to time 0)
150
100
50
0
231-mA
231-OMD
rOMD ng/mL
-
10
100
1000
231-OMD
D
231-mA
231-OMD
Control
+ 10 ng/mL rOMD
+ 100 ng/mL rOMD
+ 1000 ng/mL rOMD
1mm
E
Wound Density (%post-scratch compared to time 0)
100
50
0
MCF-7
rOMD ng/mL
-
10
100
1000
F
MCF-7
Control
+ 10 ng/mL rOMD
+ 100 ng/mL rOMD
+ 1000 ng/mL rOMD
1mm

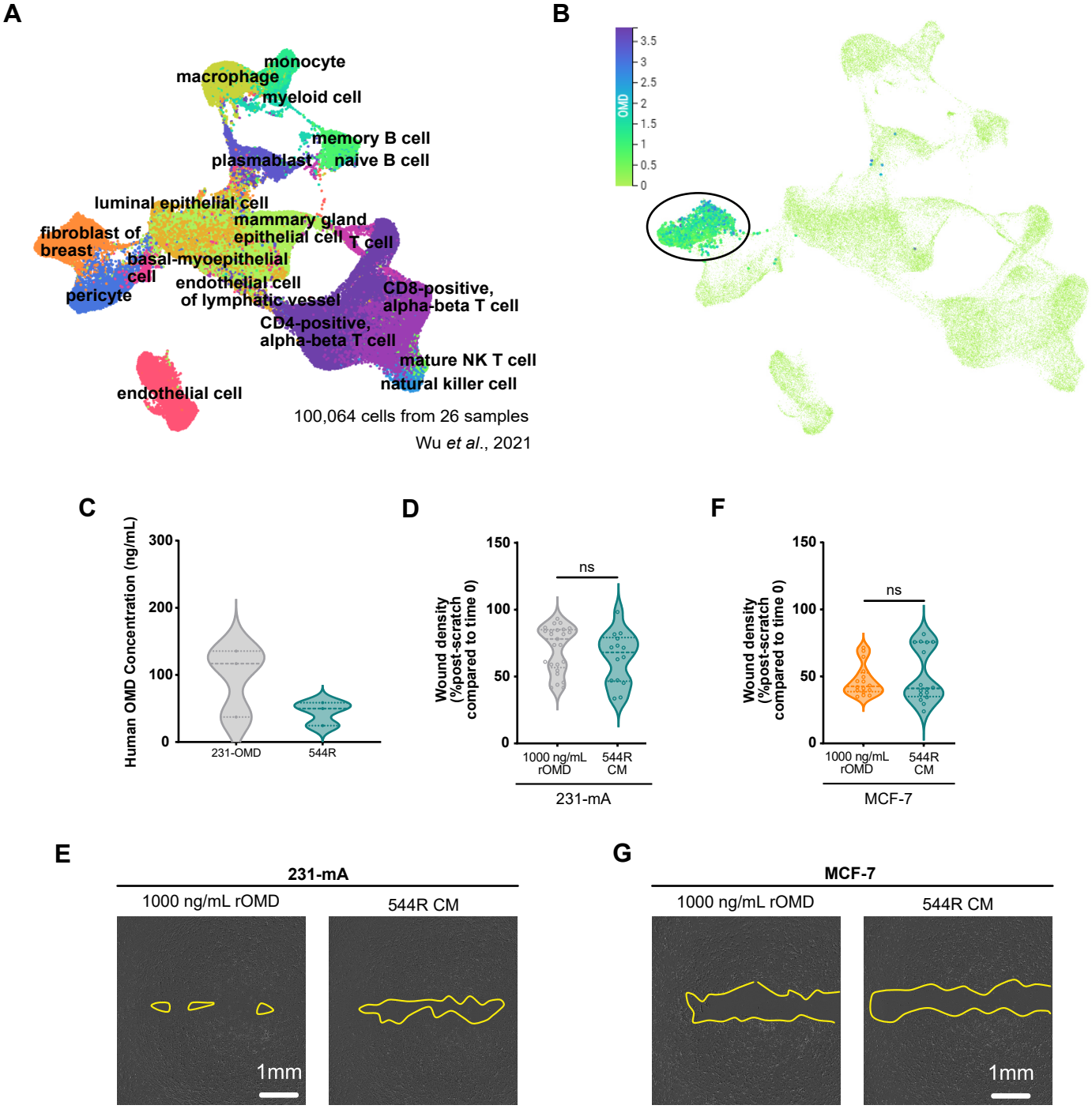
A
monocyte
macrophage
myeloid cell
memory B cell
plasmablast
naive B cell
luminal epithelial cell
mammary gland
epithelial cell
T cell
fibroblast of
breast
basal-myoepithelial
cell
endothelial cell
of lymphatic vessel
pericyte
CD8-positive,
alpha-beta T cell
CD4-positive,
alpha-beta T cell
mature NK T cell
natural killer cell
endothelial cell
100,064 cells from 26 samples
Wu et al., 2021
B
OMD
3.5
3
2.5
2
1.5
1
0.5
0
C
Human OMD Concentration (ng/mL)
300
200
100
0
231-OMD
544R
D
Wound density
(%post-scratch
compared to time 0)
150
100
50
0
ns
1000 ng/mL
rOMD
544R
CM
231-mA
F
Wound density
(%post-scratch
compared to time 0)
150
100
50
0
ns
1000 ng/mL
rOMD
544R
CM
MCF-7
E
231-mA
1000 ng/mL rOMD
544R CM
1mm
G
MCF-7
1000 ng/mL rOMD
544R CM
1mm

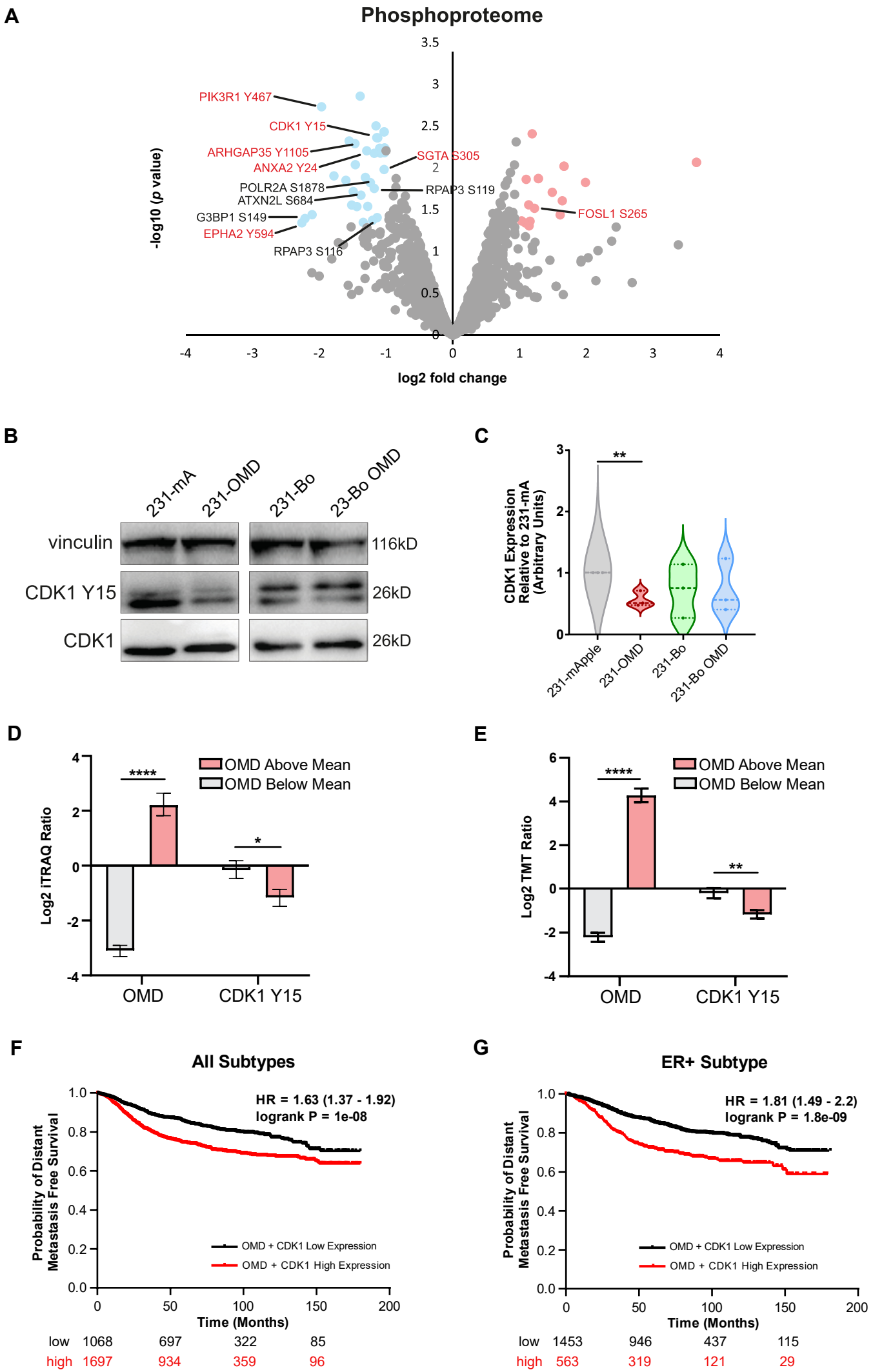
A
Phosphoproteome
PIK3R1 Y467
CDK1 Y15
ARHGAP35 Y1105
ANXA2 Y24
POLR2A S1878
ATXN2L S684
G3BP1 S149
EPHA2 Y594
RPAP3 S116
SGTA S305
RPAP3 S119
FOSL1 S265
-log10 (p value)
log2 fold change
B
231-mA
231-OMD
231-Bo
23-Bo OMD
vinculin
CDK1 Y15
CDK1
116kD
26kD
26kD
C
CDK1 Expression Relative to 231-mA (Arbitrary Units)
231-mApple
231-OMD
231-Bo
231-Bo OMD
D
OMD Above Mean
OMD Below Mean
Log2 iTRAQ Ratio
OMD
CDK1 Y15
E
OMD Above Mean
OMD Below Mean
Log2 TMT Ratio
OMD
CDK1 Y15
F
All Subtypes
HR = 1.63 (1.37 - 1.92)
logrank P = 1e-08
Probability of Distant Metastasis Free Survival
OMD + CDK1 Low Expression
OMD + CDK1 High Expression
Time (Months)
low 1068 697 322 85
high 1697 934 359 96
G
ER+ Subtype
HR = 1.81 (1.49 - 2.2)
logrank P = 1.8e-09
Probability of Distant Metastasis Free Survival
OMD + CDK1 Low Expression
OMD + CDK1 High Expression
Time (Months)
low 1453 946 437 115
high 563 319 121 29

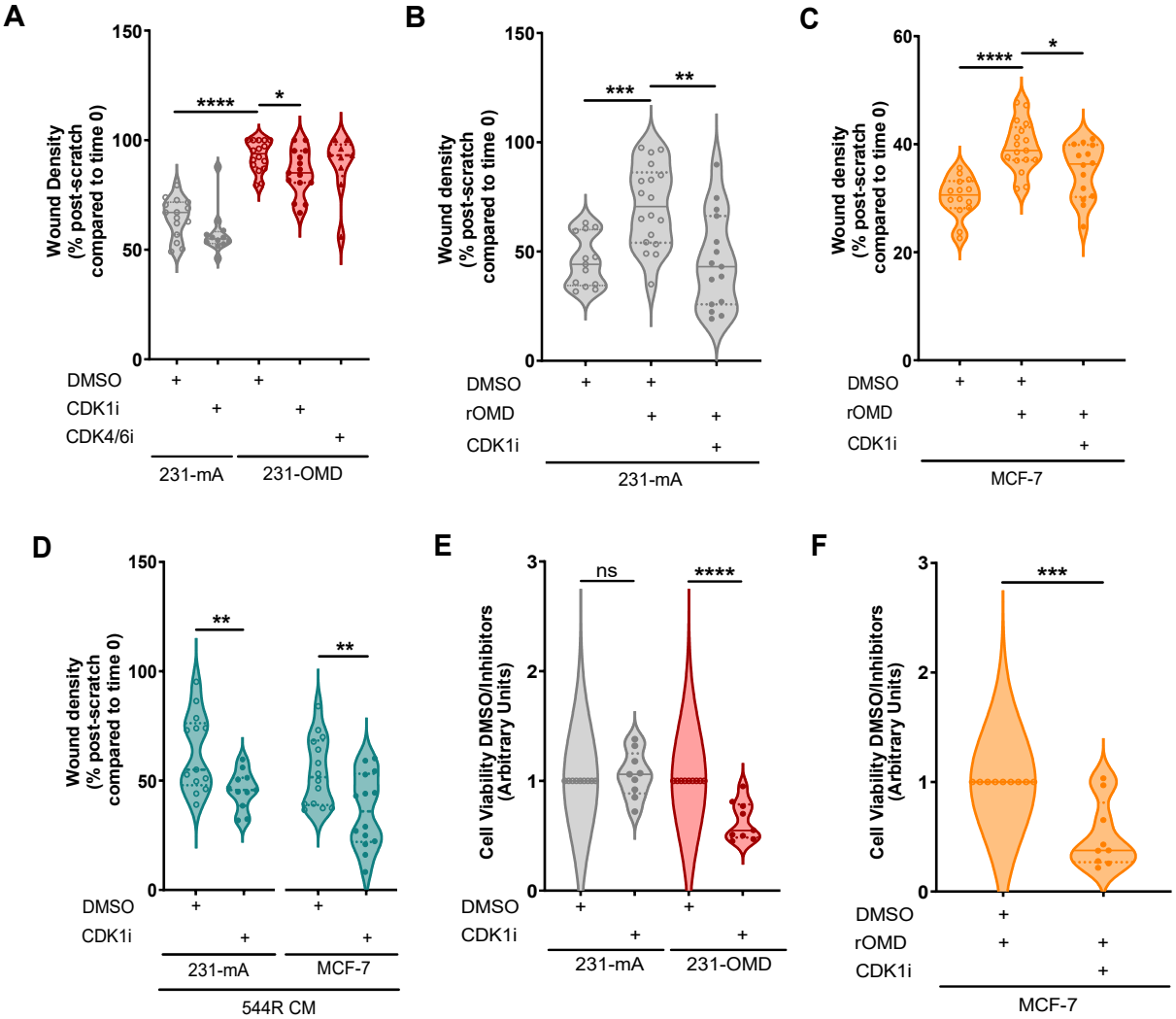

G

Sample ID	Sample Type	Tumour pathology			Sites of metastases at time of collection
		ER	PR	HER2	
BB3RC50	Ascitic Drain	+	+	-	Bone, Liver, Ovary
BB3RC82	Ascitic Drain	+	+	-	Bone
BB3RC90	Ascitic Drain	+	+	-	Liver, Bone, Pleura
BB7210 (T1, T3)	Ascitic Drain	+	+	+	Bone
BB7276	Ascitic Drain	+	+	+	Bone

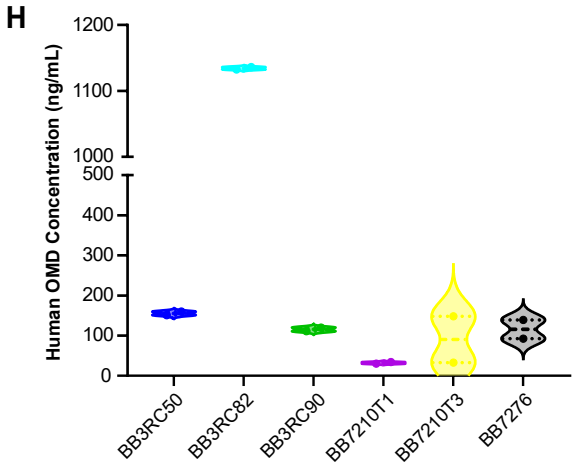

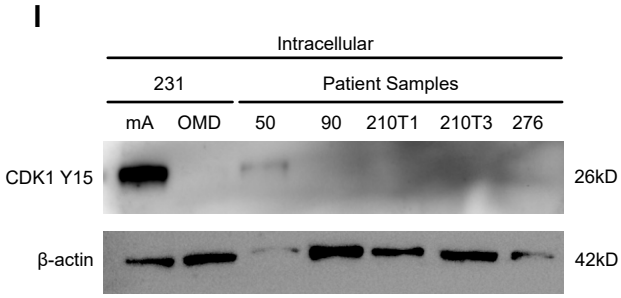

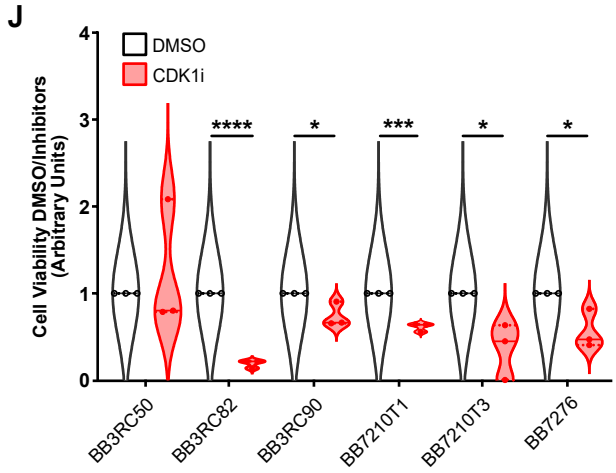

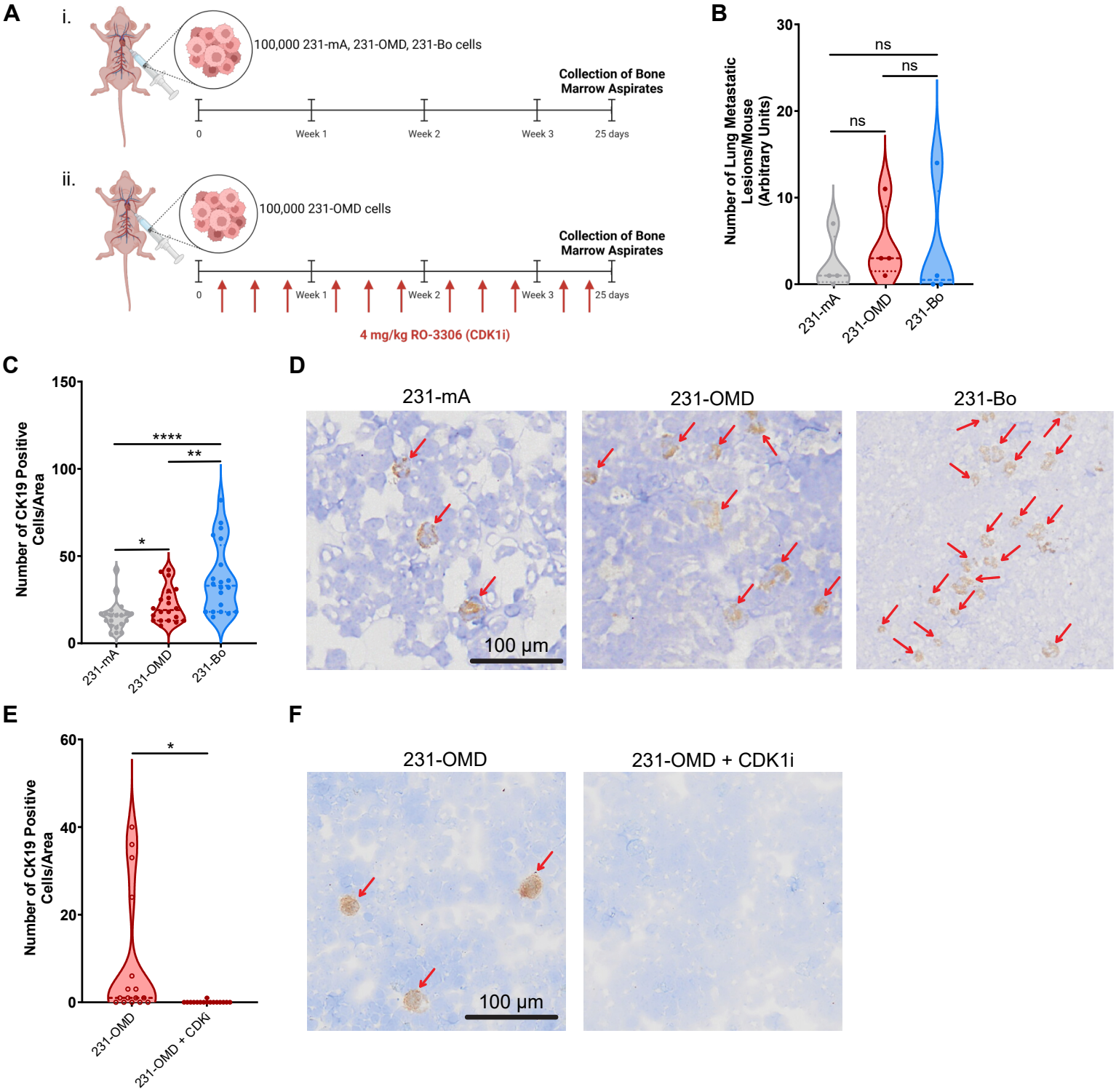
A
i.
100,000 231-mA, 231-OMD, 231-Bo cells
Collection of Bone Marrow Aspirates
0
Week 1
Week 2
Week 3
25 days
ii.
100,000 231-OMD cells
Collection of Bone Marrow Aspirates
0
Week 1
Week 2
Week 3
25 days
4 mg/kg RO-3306 (CDK1i)
B
Number of Lung Metastatic Lesions/Mouse (Arbitrary Units)
30
20
10
0
ns
ns
ns
231-mA
231-OMD
231-Bo
C
Number of CK19 Positive Cells/Area
150
100
50
0
****
**
*
231-mA
231-OMD
231-Bo
D
231-mA
231-OMD
231-Bo
100 µm
E
Number of CK19 Positive Cells/Area
60
40
20
0
*
231-OMD
231-OMD + CDKi
F
231-OMD
231-OMD + CDK1i
100 µm